

Weyl fermions with arbitrary monopole in magnetic fields: Landau levels, longitudinal magnetotransport, and density-wave ordering

Xiao Li,^{*} Bitan Roy,[†] and S. Das Sarma

Condensed Matter Theory Center and Joint Quantum Institute,
University of Maryland, College Park, MD 20742, USA

(Dated: September 1, 2022)

We theoretically address the effects of strong magnetic fields in three-dimensional Weyl semimetals (WSMs) built out of Weyl nodes with a monopole charge n . For $n = 1, 2$ and 3 we realize single, double, and triple WSM, respectively and the monopole charge n determines the integer topological invariant of the Weyl systems. Within the linearized continuum description, the quasi-particle spectrum is then composed of Landau levels (LLs), containing exactly n number of chiral zeroth Landau levels (ZLLs), irrespective of the orientation of the magnetic field. In the presence of strong backscattering (due to impurities), these systems generically give rise to longitudinal magnetotransport. Restricting ourselves to the quantum limit (and assuming only the subspace of the ZLLs is partially filled) and mainly accounting for Gaussian impurities, we show that the longitudinal magnetoconductivity (LMC) in all members of the Weyl family displays a positive linear- B scaling, when the field is applied along the axis that separates the Weyl nodes. But, in double and triple WSM, LMC displays a smooth crossover to a nonlinear B -dependence as the field is tilted away from such a high symmetry direction. In addition, due to the enhanced density of states, the LL quantization can trigger instabilities toward the formation of translational symmetry breaking density-wave orderings for sufficiently weak interaction (BCS instability), which gaps out the ZLLs. Concomitantly as the temperature (magnetic field) is gradually decreased (increased) the LMC becomes negative. Thus WSMs with arbitrary monopole charge (n) can host an intriguing interplay of LL quantization, longitudinal magnetotransport (a possible manifestation of one-dimensional chiral or axial anomaly), and density-wave ordering, when placed in a strong magnetic field.

I. INTRODUCTION

Strong spin-orbit coupling is the fundamental origin of several topological phases of matter, such as topological insulators and superconductors in two and three spatial dimensions [1–6]. The salient features of these systems are (i) an insulating bulk (electrical or thermal) and (ii) topologically protected metallic surface states. The new members of the topological family also covet surface states just like their insulating cousins, despite being characterized by gapless or non-insulating (electrical or thermal) bulk. Among such gapless phases, the ones constituted by chiral Weyl fermions have attracted considerable recent attention and may as well serve as the ideal platform where various exotic phenomena (such as axionic electrodynamics and chiral anomaly), which were originally proposed in the context of high energy physics and quantum field theory, may curve their path through the land of solid state compounds [7–9]. The current work is a comprehensive theoretical study of the strong-field longitudinal magnetotransport (LMT) properties of generalized three-dimensional Weyl systems (with arbitrary monopole charges) in the quantum limit that possibly manifests one-dimensional chiral or axial anomaly.

Weyl fermions may result from complex band structures in strong spin-orbit coupled semiconductors [10–

24], multilayer heterostructure [25–30] and they can also be found inside a broken symmetry phase in strongly correlated materials, such as 227 pyrochlore iridates, as emergent quasiparticles [31–34]. The Weyl semimetals (WSMs) can be classified into two broad categories. (i) Inversion (\mathcal{P}) symmetry breaking WSMs that are commonly found in weakly correlated semiconductors, and (ii) time-reversal (\mathcal{T}) odd WSMs that on the other hand can be found in strongly correlated materials with comparable strength of spin-orbit coupling and electronic interaction. However, irrespective of the microscopic origin, WSMs are composed of Weyl nodes in the reciprocal space, where Kramers non-degenerate valence and conduction bands touch each other at the so-called diabolic points in the momentum space [35]. The Weyl nodes act as the source (monopole) and sink (anti-monopole) of Abelian Berry flux, and in its close vicinity, Weyl fermions can be identified as left (right) chiral fermions. A *no-go theorem* guarantees the existence of an equal number of left and right chiral fermions in the system [36]. The monopole charge (n) also dictates the amount of Berry flux enclosed by a plane perpendicular to the line joining these two points and in turn defines the *integer topological invariant* of the system. Thus monopole charge permits a topological classification of Weyl semimetals, and for $n = 1, 2$ and 3 we can call them single, double and triple WSM, respectively. The dispersion of Weyl quasiparticles in these systems along various high symmetry directions is shown in Fig. 1. Although the Weyl nodes are often accompanied by *unit* monopole charge, it is nonetheless conceivable to realize

^{*}Electronic address: lixiao@umd.edu

[†]Electronic address: broy@umd.edu

Weyl nodes with higher integer charge and the system with arbitrary n can be regarded as a generalized Weyl system, such as the proposed double WSM in HgCr_2Se_4 and SrSi_2 [37–39]. Even though, the material existence of a triple WSM has remained elusive so far, with the anticipated progress of material science the discovery of such a peculiar system is certainly possible. It is well known that Weyl systems with monopole charge $n > 3$ is not allowed in three-dimensional lattice systems [38], and therefore our work applies to all possible physical Weyl materials that can be studied in the laboratory. Most, if essentially not all, of the substantial theoretical literature on WSMs have focused on the single WSM mainly because of its abundance material realization. On the other hand, there are significant differences in the properties of generalized WSMs depending on their monopole charges, necessitating theoretical studies of multi- WSMs with higher ($n > 1$) values of monopole charges.

The integer topological invariant also determines various thermodynamic, transport, and topological properties of a WSM. For example, one of the hallmark signatures of a WSM is the presence of topologically protected *Fermi arc* [31] that has recently been seen through angle resolved photoemission spectroscopy (ARPES) and scanning tunneling microscopy (STM) measurements [12, 14–19]. In a multi-WSM the Fermi arc bears additional n fold degeneracy, where n is the monopole charge of Weyl nodes. Therefore, in double and triple WSMs, the Fermi arc respectively possesses two and three fold orbital degeneracies, which, for example, can be detected in ARPES and STM. We here explore the ramifications of the underlying topological invariant of a pristine WSM, when the system is placed in a strong magnetic field. Our findings are the following.

1. When placed in a strong magnetic field, WSMs undergo Landau level (LL) quantization, supporting *exactly* n number of zeroth Landau levels (ZLLs), irrespective of the field orientation (within continuum approximation). All LLs, including the zeroth ones, disperse along the direction of the applied field. Thus, the orbital degeneracy of ZLL (n) gets tied with the monopole charge or topological invariant of the Weyl nodes.
2. Even though n dispersive ZLLs always go through zero energy (in the continuum limit), they are in general non-degenerate, unless the field is applied along the axis on which Weyl nodes reside in the absence of the field [see Figs. 5(a) and 5(b)].
3. Density of states (DOS) displays nontrivial dependence (such as its periodicity) on the tilting angle of the magnetic field away from a high symmetry direction, separating the Weyl nodes [see Figs. 6 and 7]. Such intriguing features can be observed in *angle resolved* quantum oscillation measurements [40, 41].

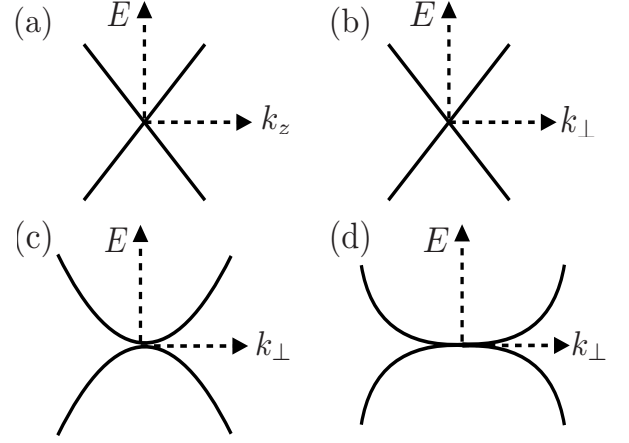


FIG. 1: (a) Spectrum of Weyl fermions along the k_z direction in any Weyl semimetal. Dispersion in the xy plane respectively for (b) single, (c) double and (d) triple Weyl semimetals. Notice that $E \sim |\mathbf{k}_\perp|^n$, where n is the monopole charge and $\mathbf{k}_\perp = (k_x, k_y)$, but $E \sim |k_z|$ in all Weyl semimetals.

A strong magnetic field causes an *effective* reduction of the dimensionality of the system. In particular, each branch of ZLLs cuts the zero energy (where the Fermi energy is pinned) at two isolated points in the Brillouin zone, yielding two field-induced Weyl nodes, around which the quasiparticles are once again described as one-dimensional chiral (left and right) fermions. If an electric field (E) is now applied in parallel to the magnetic field, it can cause charge transfer from left to right Weyl nodes, causing *violation of separate conservation laws for left and right chiral fermions*, captured by the following anomaly equation [42, 43]

$$\partial_\mu (j_{\mu,R} - j_{\mu,L}) = N \frac{eE}{\hbar\pi}. \quad (1)$$

Here, e is the electric charge, $j_{\mu,R/L}$ is the charge (for $\mu = 0$) and current (for $\mu = j = 1$) operator for left/right chiral fermion, and N can be identified as the total degeneracy of effective one-dimensional system. The total charge and current density is respectively given by $j_0 = \Psi^\dagger \Psi$ and $j_1 = \Psi^\dagger \sigma_3 \Psi$, where $\Psi^\top = (\Psi_L, \Psi_R)$ is a two component spinor, describing the emergent one-dimensional world. Due to the reduced dimensionality of the system, one can define $\sigma_3 \equiv \gamma_5$, and accordingly we can define axial or chiral charge and current density as $j_0^{ax} = \Psi^\dagger \gamma_5 \Psi = j_1$ and $j_1^{ax} = \Psi^\dagger \Psi = j_0$. Hence, one can express Eq. (1) as $\partial_\mu j_\mu^{ax} = N(eE)/(\hbar\pi)$. In the language of quantum field theory, such violation of separate conservation laws for left and right fermions is known as *chiral anomaly*, specific to odd spatial dimensions. In regular WSM, the degeneracy of the ZLL plays the role of N , whereas in WSMs with $n \neq 1$, $N = n \times \text{LL degeneracy}$. Therefore, upon identifying N as the *total* degeneracy of ZLL, we arrive at the celebrated *Adler-Jackiw-Bell*

anomaly equation [42, 44, 45]

$$\partial_\mu j_\mu^{ax} = n \frac{e^2}{2\pi^2\hbar} \mathbf{E} \cdot \mathbf{B}, \quad (2)$$

now generalized for a Weyl system, constituted by Weyl nodes with monopole charge n . Notice that here electric (\mathbf{E}) and magnetic (\mathbf{B}) fields are strictly *static Abelian background fields*. We also stress that in the above expression $\mathbf{E} \cdot \mathbf{B}$ can *never* be negative as the B -linear dependence arises from the LL DOS, and insensitive to the direction of applied electric and magnetic field.

Such analogy, undoubtedly tantalizing and recently led to a culmination of theoretical [46–68] and experimental [69–82] activities aimed toward demonstrating manifestation of chiral anomaly through LMT, nevertheless raises a concern regarding its jurisdiction in solid state materials since the nonconservation chiral current crucially depends on the existence of an *unbounded* linear dispersion of Weyl fermions [42–45], whereas the energy dispersion in all condensed matter systems is unavoidably bounded by the natural lattice cut off. However in a pioneer work Nielsen and Ninomiya showed that certain gapless semiconductors accommodating linear touching of valence and conduction bands can give rise to LMT [83]. In this regard, we must recall that almost thirty years before the proposal of Nielsen and Ninomiya, Adam and Argyres demonstrated the existence of LMT for conventional three-dimensional isotropic Fermi liquids without invoking the notion of chiral or axial anomaly [84]. Their derivation of LMT solely relies on few generic features of a three-dimensional electronic system in a strong magnetic field: the existence of (i) one-dimensional dispersive LLs since momentum along the applied magnetic field is a conserved quantity, and (ii) at least one partially filled LL that cuts Fermi energy at two isolated points (or in general even number of points in the Brillouin zone). Therefore, the existence of LMT in the absence of the classical Lorentz force (when \mathbf{E} and \mathbf{B} are parallel) although necessarily points toward subtle quantum mechanical effects, yet its direct connection with chiral anomaly is not obvious. Recently Goswami *et al.* in Ref. [85] have demonstrated the generic existence of LMT for “a generic three dimensional metal”. Specifically, the chiral anomaly implies an LMT through the *Nielsen-Ninomiya mechanism*, but the reverse remains to be established. We here follow the philosophy of Ref. [84] and show that WSM with arbitrary monopole charge display LMT when placed in a strong magnetic field. For the sake of technical simplicity we assume that only the manifold of ZLLs is partially filled. However, our analysis can be generalized to demonstrate generic LMT in Weyl materials even when multiple LLs are partially filled (see Sec. V E). The possibility that the strong-field positive magnetoconductance in electronic materials is a generic phenomenon associated with LL impurity scattering has recently received compelling support from experimental works [72, 82], making our current theoretical quest into the LMC for generalized WSMs particularly timely and

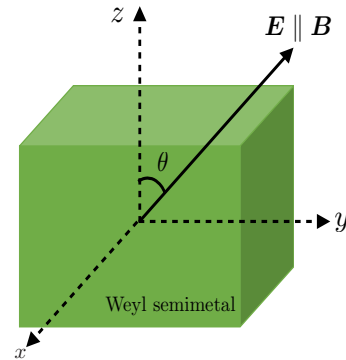


FIG. 2: (Color online) Schematic representation of the applied electric (\mathbf{E}) and magnetic (\mathbf{B}) fields (always parallel). Quasi-particle dispersion along z direction is $v_z k_z$, while in the xy plane is proportional to $|k_\perp|^{n/2}$, where $\mathbf{k}_\perp = (k_x, k_y)$. Here, θ parametrizes the tilting of magnetic field away from the z direction. Weyl nodes are separated along the z direction.

relevant.

In this context few comments are due. In the presence of the periodic potential in a solid, arising from ionic lattice, quasiparticles perform Bloch oscillations and consequently the system cannot sustain any finite steady state current [86]. Nevertheless, in the presence of relaxation mechanism, which is naturally offered by impurities, quasiparticles lose the freedom to perform a complete Bloch oscillation and a metallic system can support finite steady state current, when the relaxation or transport lifetime (τ) is much shorter than the Bloch oscillation period. In this work, we focus on the low temperature situation where impurity scattering is the primary scattering mechanism for transport as phonons are mostly frozen out. Furthermore, in the presence of strong magnetic fields, i.e. when $\omega_c \tau \gg 1$ where ω_c is the cyclotron frequency, the path of the carriers is so curved that the period of completing a cyclotron orbit becomes comparable to that between two successive collisions. Therefore, the transport/relaxation time acquires a strong field dependence and $\tau = \tau(B)$. Such a field dependence of τ is extracted here by using *quantum Boltzmann equation*, but omitted in the semiclassical theory, which therefore is only applicable for extremely weak magnetic fields ($\omega_c \tau \ll 1$). But, for sufficiently weak magnetic fields one needs to account for yet another pure quantum mechanical effect, the *weak localization* [87, 88]. Presently it is unknown how to incorporate all these effects in a unified theoretical framework, and restricting ourselves to the strong field quantum limit $\omega_c \tau \gg 1$ we establish the followings:

1. In the presence of both Gaussian and Coulomb impurities, we extract the magnetic field dependence of transport lifetime using quantum Boltzmann equation, and show that all WSMs manifest *positive* longitudinal magnetoconductivity (LMC) or negative longitudinal magnetoresistivity (LMR),

when the magnetic and electric fields are applied parallel to each other (see Fig. 2).

2. Due to the carrier-induced screening of Coulomb potential (arising from finite DOS of LLs), we mainly focus on Gaussian impurities and show that when the fields are applied along a high symmetry axis separating the Weyl nodes, the LMC increases linearly with B in all WSMs (see Fig. 8). The LMC in the presence of only Coulomb impurities grows as B^2 , but only in extreme strong field limit.
3. Although such a linear increase of LMC is insensitive to the field orientation in single WSMs, LMC develops *nonlinear* dependencies on the magnetic field in double and triple WSM when the field is tilted away from the high symmetry axis (see Figs. 9 and 10), which can be tested in proposed double WSMs HgCr_2Se_4 and SrSi_2 .

We find that typically the relaxation lifetime due to Gaussian impurities $\tau_G \ll \tau_C$, where τ_C is the same quantity but due to ionic impurities. Hence, the transport lifetime is dominated by Gaussian impurities and in our analysis we mainly focus on short range elastic scatterer. In addition, We also investigate the role of electronic interaction on LMT as the temperature (magnetic field) is gradually decreased (increased). The DOS in a pristine WSM scales as $E^{2/n}$ and the Weyl nodes are extremely robust against weak short-range electron-electron interaction. However, due to Landau quantization, the DOS for the emergent one-dimensional world is *constant*, which in turn can trigger various density-wave instabilities even when the electronic interaction is sufficiently weak. The quintessential effects of interactions can be summarized as the following.

1. Depending on the microscopic details, ZLLs can undergo a weak coupling (BCS-like) instability in the charge-density-wave (CDW) or spin-density-wave (SDW) channel. Irrespective of the actual nature of the ordering the density-wave orders break the translational symmetry and gap out the ZLLs.
2. When the field is applied along the high symmetry axis all n number of ZLLs are expected to suffer density-wave ordering *simultaneously*. Thus, below the transition temperature (T_c) LMC (LMR) becomes *negative (positive)*, reversing the trend compared with the normal phase with no density wave ordering. However, upon tilting the field away from the high symmetry axis, the exact n fold degeneracy of ZLLs is lifted, and the system can undergo a *cascade* of density-wave transitions with distinct transition temperatures. Hence, LMC/LMR in a multi-WSM is expected to display n fold discontinuity before it becomes negative/positive.

Although such ordering in a clean system (devoid of any impurity) should take place for arbitrarily weak

interaction, disorder naturally reduces the propensity towards such translational symmetry breaking ordering [89]. Thus clear signatures of CDW or SDW ordering can only be observed in clean systems at sufficiently low temperature and for strong enough magnetic fields.

The rest of the paper is organized in the following way. In Sec. II, we discuss the possibility of realizing Weyl semimetals with different monopole charge and address their topological properties (such as bulk-boundary correspondence through degeneracy of Fermi arc). Sec. III is devoted to the demonstration of LL spectra in single, double and triple WSMs for arbitrary orientation of the magnetic field. DOS in these systems in the presence of strong magnetic field is presented in Sec. IV. Longitudinal magnetotransport for all members of the Weyl family constitutes the central theme of Sec. V. Effects of various density-wave ordering on LMT are discussed in Sec. VI. We summarize the main findings in Sec. VII. Some technical details are relegated to Appendices.

II. WEYL SEMIMETALS: A GENERAL CONSTRUCTION AND TOPOLOGY

A WSM is realized when a solid state system lacks inversion and/or time-reversal symmetry, and the Kramers non-degenerate valence and conduction bands touch each other at isolated points in the Brillouin zone, known as Weyl nodes. The simplest realization (composed of only two Weyl points) arises from the following tight-binding model in a cubic lattice

$$H = \sum_{\mathbf{k}} \Psi_{\mathbf{k}}^\dagger [\sigma_1 N_1(\mathbf{k}_\perp) + \sigma_2 N_2(\mathbf{k}_\perp) + \sigma_3 N_3(\mathbf{k})] \Psi_{\mathbf{k}}, \quad (3)$$

where $\mathbf{k}_\perp = (k_x, k_y)$, $\Psi^\top(\mathbf{k}) = (c_{\uparrow, \mathbf{k}}, c_{\downarrow, \mathbf{k}})$ is a two component spinor and σ s are three Pauli matrices. With the following choice

$$N_3(\mathbf{k}) = -t[2 - \cos(k_x a) - \cos(k_y a)] - t \cos(k_z a) + m_z, \quad (4)$$

where a is the lattice spacing, two Weyl nodes are located along one of the C_{4v} axes, namely at $k_z = \pm \cos^{-1}[m_z/(t_z a)]$. Now, if we choose $N_1(\mathbf{k}) = t \sin(k_x a)$ and $N_2(\mathbf{k}) = t \sin(k_y a)$, two Weyl nodes with monopole charge ± 1 are realized at $\pm K_0$, where $K_0 = (0, 0, \cos^{-1}[m_z/(t_z a)])$. The linearized Hamiltonian for single WSM in the vicinity of the $\Gamma = (0, 0, 0)$ point is

$$H_1 = \hbar(v_x \sigma_1 k_x + v_y \sigma_2 k_y) - \sigma_3 \frac{\hbar^2 (k_z^2 + k_\perp^2)}{2m} + \Delta, \quad (5)$$

where v_{js} are the Fermi velocity of Weyl quasiparticles, $v_x = v_y = ta$, $m^{-1} = ta^2$, $\Delta = m_z - t$, and the momentum (\mathbf{k}) is measured from the Γ points. In the close proximity to these two Weyl points the low energy excitations are respectively described by left and right chiral fermion, constituting source and sink of the Abelian Berry curvature, respectively. In an appropriate crystallographic

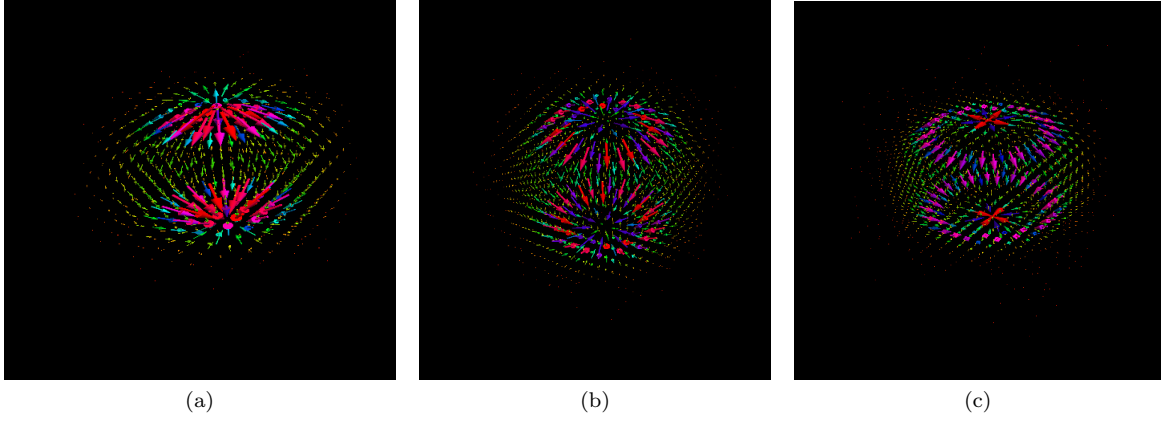


FIG. 3: (Color online) Vector field plots for the Berry curvature for Weyl fermion, (a) when the Weyl nodes are monopole (source) and anti-monopole (sink) of Berry curvature, with unit charge. In double and triple WSMs the Weyl nodes are source and sink of Berry curvature with charge two and three, respectively, and the vector field plots are shown in panel (b) and (c).

environment it is also conceivable to realize Weyl points with higher monopole charge [37]. In particular Weyl nodes with monopole charge *two* and *three* can respectively be stabilized when the underlying lattice possesses tetragonal C_{4v} and C_{6v} symmetries, respectively [37, 38]. A double WSM, for example, can be realized from Eq. (3) by choosing $N_1(\mathbf{k}) = t[\cos(k_x a) - \cos(k_y a)]$, $N_2(\mathbf{k}) = t \sin(k_x a) \sin(k_y a)$, while leaving $N_3(\mathbf{k})$ unchanged [90]. But, in three spatial dimensions it is impossible to realize Weyl nodes with monopole charge larger than three from an underlying lattice model.

The above construction can also be viewed in the following way that will allow us to identify the topological invariant of these systems. Note that WSMs can be constructed by appropriately stacking two-dimensional layers of *quantum anomalous Hall insulators* (QAHI) in the Brillouin zone along the k_z -direction. A two-dimensional QAHI supports quantized Hall conductivity $\sigma_{xy} = ne^2/h$, where n represents the number of one-dimensional chiral edge states. For each k_z , satisfying $-\frac{\sqrt{2m\Delta}}{\hbar} < k_z < \frac{\sqrt{2m\Delta}}{\hbar}$, the pseudospin texture is *skyrmion*, with skyrmion number n , and two Weyl nodes appear as *singularities* in the Brillouin zone, across which the skyrmion number *jumps* by $\pm n$. When stacked along the k_z direction, the chiral edge modes from two-dimensional layers of QAHI produce the Fermi arc, *possessing n -fold orbital degeneracy*. The topological invariant of a WSM can be assessed from the gauge invariant Berry curvature defined as [91]

$$\Omega_{n,\mathbf{k},a} = \frac{(-1)^n}{4} \epsilon_{abc} \mathbf{n}_{\mathbf{k}} \cdot \left[\frac{\partial \mathbf{n}_{\mathbf{k}}}{\partial k_b} \times \frac{\partial \mathbf{n}_{\mathbf{k}}}{\partial k_c} \right], \quad (6)$$

where $\mathbf{n}_{\mathbf{k}} = \mathbf{N}_{\mathbf{k}}/|\mathbf{N}_{\mathbf{k}}|$, and $n = \pm$ corresponds to valence and conduction band, respectively. Upon evaluating the components of the Abelian Berry curvature we plot it in Figs. 3(a), 3(b) and 3(c) respectively for single, double and triple WSM. The components of Berry curvature $\Omega_{n,\mathbf{k},x}$ and $\Omega_{n,\mathbf{k},y}$ are odd function of k_x and k_y respec-

tively. Hence, the number of field lines coming in and out of the xz or yz planes are equal, and the net Berry flux through these planes is zero. On the other hand, $\Omega_{n,\mathbf{k},z}$ is an even function of \mathbf{k} and the net Berry flux through the xy plane is $2\pi\mathcal{S}(k_z)$, where $\mathcal{S}(k_z)$ is the Chern number of effective two-dimensional system for a fixed k_z . For $-\frac{\sqrt{2m\Delta}}{\hbar} < k_z < \frac{\sqrt{2m\Delta}}{\hbar}$, $\mathcal{S}(k_z) = n$, while $\mathcal{S}(k_z) = 0$ when $|k_z| > \frac{\sqrt{2m\Delta}}{\hbar}$. Therefore, two Weyl points in a general WSM act as source and sink of Abelian Berry curvature, across which the Chern number of the underlying two-dimensional system jumps by an integer amount n .

In the low energy limit the Hamiltonian for an WSM, constituted by Weyl nodes with monopole charge $\pm n$ is compactly written as

$$H_{\pm n} = \begin{pmatrix} \pm v_z \hbar k_z + \frac{\hbar^2 k_{\perp}^2}{2m} & \alpha_n (\hbar k_{\perp})^n e^{-in\theta_k} \\ \alpha_n (\hbar k_{\perp})^n e^{in\theta_k} & \mp v_z \hbar k_z - \frac{\hbar^2 k_{\perp}^2}{2m} \end{pmatrix}, \quad (7)$$

after linearizing the generalized version of the Hamiltonian from Eq. (5) for general WSM around $\pm k_z^0$, where $k_z^0 = \sqrt{2m\Delta}$. In the above equation, therefore, k_z is measured from $\pm k_z^0$. Thus, α_1 and α_2 respectively bear the unit of Fermi velocity and inverse of mass.

The majority of the known Weyl materials only break the inversion symmetry and the Weyl nodes are placed at different energies. Notice that the WSM arising from the tight-binding model, defined in Eq. (3), breaks both time-reversal and inversion symmetries, but the Weyl nodes are still located at the same energy. With simple modifications in this tight-binding model, for example by adding a term $[\Delta_0 + \Delta_{ch} \sin(k_z c)]\sigma_0$ to Eq.(3), the Weyl nodes can be placed at different energies, namely at $\Delta_0 \pm \Delta_{ch}$. Here, Δ_0 and Δ_{ch} are respectively regular and chiral chemical potentials. However, our following discussion on various aspects of Weyl fermions in a strong magnetic field is qualitatively insensitive to such details of the system. Next we demonstrate how the underlying topological invariant of a WSM manifests through

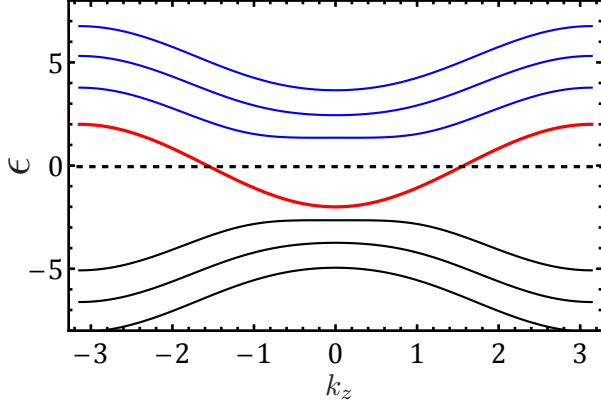


FIG. 4: (Color online) Landau level (LL) spectrum in single Weyl semimetal, obtained from Eq. (7) when $n = 1$. For details see Appendix A. Here the zeroth LL (red curve) is non-degenerate, and the energy ϵ (in units of $2\alpha_1^2\hbar^2/\ell_B^2$) is measured about a reference or zero point energy $\hbar^2/(2m\ell_B^2)$. At half-filling the zeroth LL cuts the Fermi energy (dotted line) at $k_z = \pm\pi/(2a)$ (we set $a = 1$ for convenience) [85]. Similar LL spectrum is found for double and triple Weyl semimetals, for which, however, the zeroth LL has two and three fold degeneracy, respectively.

the LL spectrum when the system is subject to a strong magnetic field.

III. LANDAU LEVELS

Effects of the magnetic field applied in an arbitrary direction, can be captured through minimal coupling $\mathbf{k} \rightarrow \mathbf{k} - e\mathbf{A} \equiv \boldsymbol{\pi}$, where \mathbf{A} is the vector potential, e is electronic charge and the magnetic field is given by $\mathbf{B} = \nabla \times \mathbf{A}$. Before delving with the situation when the magnetic field is tilted away from the z direction (parametrized by θ , see Fig. 2), let us first focus on a simpler situation when the field is applied along the z -direction, i.e. $\mathbf{B} = (0, 0, 1)B$, for which momentum k_z is a conserved quantity. We can analytically obtain the LL spectrum [92, 93]. For simplicity, we work with the Landau gauge $\mathbf{A} = (0, Bx, 0)$, and define the raising and lowering operators as $a = \ell(\pi_x - i\pi_y)/(\sqrt{2}\hbar)$ and $a^\dagger = \ell(\pi_x + i\pi_y)/(\sqrt{2}\hbar)$, where $\ell = \sqrt{\hbar/eB}$ is the magnetic length, and $[\pi_x, \pi_y] = -i\hbar eB$. The low energy Hamiltonian for a general Weyl semimetal then reads as

$$H_{n,\theta=0} = \begin{pmatrix} \hbar v_z k_z & \alpha_n \frac{(\sqrt{2}\hbar a)^n}{\ell^n} \\ \alpha_n \frac{(\sqrt{2}\hbar a)^n}{\ell^n} & -\hbar v_z k_z \end{pmatrix}. \quad (8)$$

We here omit the term $\hbar^2 k_\perp^2/(2m)$ with respect to k_x and k_y for small momentum (near the Weyl nodes), mainly since inclusion of such term causes an overall shift in the

LL energy at least when $\mathbf{B} = B\hat{z}$. The LL spectrum can then be readily obtained, yielding

$$\begin{aligned} E_{s,n,m}(k_z) &= s\sqrt{v_z^2\hbar^2k_z^2 + \frac{2\hbar^2\alpha_1^2}{\ell^2}m}, \quad (m \geq 1) \\ &= s\sqrt{v_z^2\hbar^2k_z^2 + \frac{4\hbar^4\alpha_2^2}{\ell^4}m(m-1)}, \quad (m \geq 2) \\ &= s\sqrt{v_z^2\hbar^2k_z^2 + \frac{8\hbar^6\alpha_3^2}{\ell^6}m(m-1)(m-2)}, \quad (m \geq 3), \end{aligned} \quad (9)$$

for $s = \pm$ for single, double and triple WSM, respectively. For simple WSM the ZLL is comprised of a single branch with energy $E_{n=0}(k_z) = -\hbar v k_z$, while for double WSM $E_{n=0}(k_z) = E_{n=1}(k_z) = -\hbar v k_z$ and for a triple WSM $E_{n=0}(k_z) = E_{n=1}(k_z) = E_{n=2}(k_z) = -\hbar v k_z$. Thus, the ZLL for double and triple WSM enjoys additional *two* and *three* fold orbital degeneracy, respectively. We obtain exactly n number of ZLL in the presence of bounded dispersion from a lattice model, as shown in Fig. 4 when $\mathbf{B} = B\hat{z}$. Details of the calculation are provided in Appendix A. Thus, the integer topological invariant of a WSM or monopole charge of the Weyl nodes sets the orbital degeneracy of the ZLL, at least when the field is applied along the separation of the Weyl nodes. When the underlying lattice potential is taken into account, giving rise to bounded dispersion, the ZLL cuts the zero energy at $k_z = \pm\pi/(2a)$, and in the following we focus near one such Weyl point.

Next we will show that the orbital degeneracy of ZLL remains unaffected with the tilting of the magnetic field away from the z -direction ($\theta \neq 0$), at least within the continuum description. For concreteness, we take the following vector potential $\mathbf{A} = (0, Bx \cos \theta, -Bx \sin \theta)$, giving rise to $\mathbf{B} = (0, B \sin \theta, B \cos \theta)$. The commutation relations between different momentum operators are given by $[\pi_x, \pi_y] = -i\hbar eB \cos \theta$ and $[\pi_x, \pi_z] = i\hbar eB \sin \theta$. We can define a pair of raising and lowering operators as

$$\begin{aligned} a &= \frac{\ell}{\sqrt{2}\hbar}[\pi_x - i(\pi_y \cos \theta - \pi_z \sin \theta)], \\ a^\dagger &= \frac{\ell}{\sqrt{2}\hbar}[\pi_x + i(\pi_y \cos \theta - \pi_z \sin \theta)], \end{aligned} \quad (10)$$

which satisfies the standard commutation relation $[a, a^\dagger] = 1$. The momentum along the magnetic field, defined as $k_0 \equiv k_y \sin \theta + k_z \cos \theta$, is a conserved quantity, and we find

$$\begin{aligned} \pi_x &= \frac{\hbar}{\sqrt{2}\ell}(a + a^\dagger), \quad \pi_y = \hbar k_0 \sin \theta + \frac{i\hbar}{\sqrt{2}\ell}(a - a^\dagger) \cos \theta, \\ \pi_z &= \hbar k_0 \cos \theta - \frac{i\hbar}{\sqrt{2}\ell}(a - a^\dagger) \sin \theta. \end{aligned} \quad (11)$$

The LL spectrum for an arbitrary orientation of the magnetic field ($\theta \neq 0$) in a multi-WSM cannot be obtained analytically. The numerically obtained LL spectrum for double and triple WSM are respectively shown

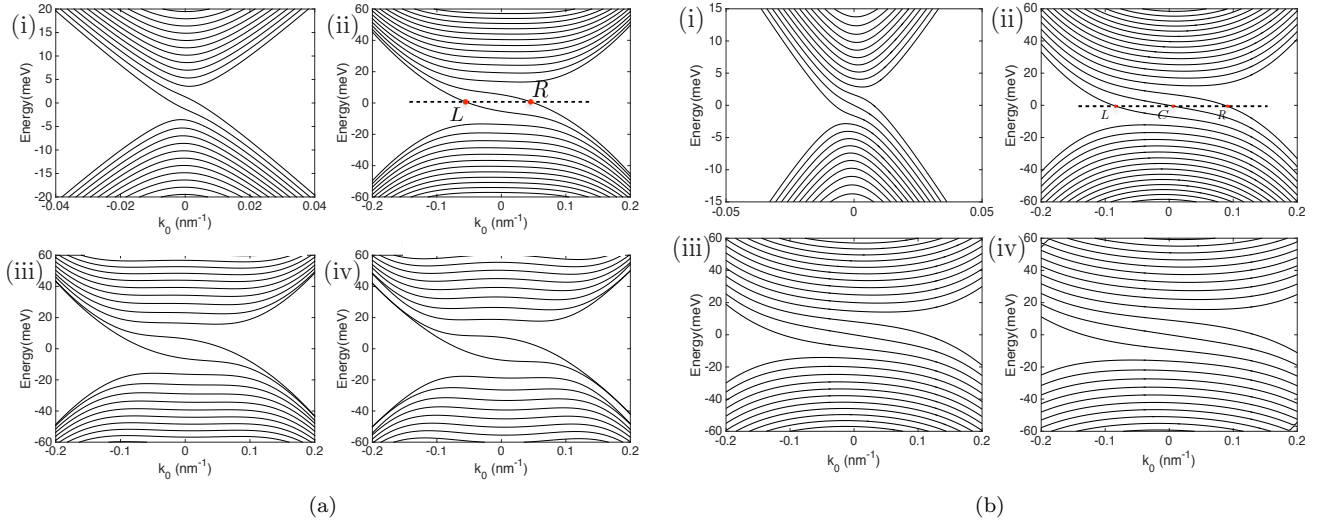


FIG. 5: (Color online) (a) Landau level spectrum for double-Weyl semimetals when the magnetic field is $B = 1$ T and the direction of applied field is characterized by (i) $\theta = 3\pi/100$, (ii) $\theta = \pi/4$, (iii) $\theta = \pi/3$, and (iv) $\theta = \pi/2$ for $v_z = 658.2$ meV·nm and $\alpha_2 = 500$ meV·nm². (b) Landau level spectrum for triple-Weyl semimetals for same orientations of the magnetic field for $v_z = 658.2$ meV·nm and $\alpha_3 = 1782.29$ meV·nm³.

in Fig. 5(a) and Fig. 5(b), for various choices of θ . For simplicity, we have only shown the LL structure near one Weyl node, hosting left chiral fermion. A similar LL structure is also realized for right chiral fermion, and all LLs (including the zeroth one) are bounded due to the underlying lattice. Therefore, when $\theta \neq 0$ the exact degeneracy among the chiral ZLLs is lifted. However, there is always n number of chiral ZLL crossing the zero energy. Such an outcome can be substantiated from the fact that in the absence of any magnetic field the monopole charge of the Weyl nodes is $\pm n$, which in turn determines the orbital degeneracy of the ZLL.

Although the LL spectrum obtained from the continuum description of WSM captures most of the essential features, a comment in this context is in order. When the field is tilted from the z direction the two copies of ZLLs in double WSM cuts the zero energy at momentum $\pm[\pi/2 \pm \delta(\theta)]a^{-1}$, where $\delta(\theta)$ is dependent on the tilting angle, as shown in Fig. 5(a), when the system is at half-filling. Similarly, in triple WSM the ZLL cuts the zero energy at $\pm[\pi/2 + j\delta(\theta)]a^{-1}$ for $j = -1, 0, 1$. In Figs. 5(a) and 5(b), the conserved momentum k_0 is measured from one of the emergent Weyl nodes in magnetic fields, located at $\pi/(2a)$. Next we discuss the resulting DOS in the presence of magnetic field.

IV. DENSITY OF STATES

It is instructive to separately study the DOS in single, double and triple WSM, when placed in a magnetic field, as it can be directly tested in angle resolved quantum oscillation measurements [40, 41]. In the presence of strong

magnetic fields the kinetic energy in the plane perpendicular to \mathbf{B} is completely quenched, while the LLs remain dispersive along the applied magnetic field. Thus the magnetic field causes an effective dimensional reduction of the system, and the WSM in the external magnetic field can be viewed as a *collection of one-dimensional systems with multiple subbands*. The DOS of such a system can be found from the following definition

$$D(\mu) = \frac{L}{2\pi} \sum_m \int_{-\infty}^{+\infty} dk \delta(E_m(k) - \mu), \quad (12)$$

where m labels different subbands, and k is the conserved momentum of the one-dimensional conducting channel, along the magnetic field direction, and L is the linear dimension along the field.

The DOS for a single WSM can be obtained in a closed-form. We first note that the dispersion for a single WSM can be cast in the following form

$$E_m(k) = \sqrt{\hbar^2 v_z^2 k^2 + w^2}, \quad (13)$$

where $w = \sqrt{m}\epsilon_1$ and $\epsilon_1 = \sqrt{2}\hbar\alpha_1/\ell$. In such a system each $m \geq 1$ LLs crosses the Fermi energy μ twice, at $k_c = \pm\sqrt{\mu^2 - w^2}/(\hbar v_z)$, whereas the $m = 0$ LL only cuts the Fermi energy once, at $k = -\mu/(\hbar v_z)$. Therefore, the DOS for this single WSM is given by

$$D(\mu) = \frac{L}{2\pi\hbar v_z} \left[1 + \sum_{m \geq 1} \frac{2\mu \Theta(\mu - \sqrt{m}\epsilon_1)}{\sqrt{\mu^2 - m\epsilon_1^2}} \right], \quad (14)$$

where $\Theta(x)$ is the Heaviside Theta function.

Similarly we can analytically find the DOS for double WSM when the field is along the k_z direction. The dispersion relation is then readily obtained from Eq. (13) after

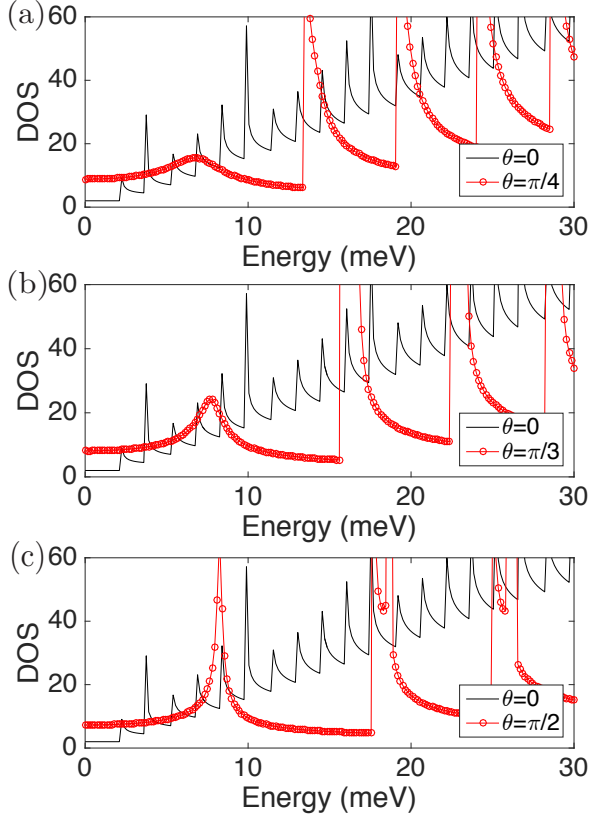


FIG. 6: (Color online) DOS for Landau levels in a double-Weyl semimetal, in units of $L/(2\pi\hbar v_z)$. The parameters are the same as those in Fig. 5(a). The black curves are the DOS when the applied magnetic field is along the z direction ($\theta = 0$), see Eq. (15).

replacing w by $w = \sqrt{m(m-1)}\epsilon_2$, where $\epsilon_2 = 2\hbar^2\alpha_2/\ell^2$, and the DOS for such a system is given by

$$D(\mu) = \frac{L}{2\pi\hbar v_z} \left[2 + \sum_{m \geq 2} \frac{2\mu \Theta(\mu - \sqrt{m(m-1)}\epsilon_2)}{\sqrt{\mu^2 - m(m-1)\epsilon_2^2}} \right], \quad (15)$$

where we have accounted for the two-fold degeneracy of the ZLL. The above expression for DOS in double WSM is plotted as black lines in Fig. 6. Similarly, it is easy to show that when the field is applied along the z direction the DOS in triple WSM is given by

$$D(\mu) = \frac{L}{2\pi\hbar v_z} \left[3 + \sum_{m \geq 3} \frac{2\mu \Theta(\mu - \sqrt{m(m-1)(m-2)}\epsilon_3)}{\sqrt{\mu^2 - m(m-1)(m-2)\epsilon_3^2}} \right] \quad (16)$$

where $\epsilon_3 = (\sqrt{2}\hbar)^3\alpha_3/\ell^3$, as shown by the black lines in Fig. 7.

For arbitrary orientations of the magnetic field, we compute the DOS numerically. In Fig. 6 we display the DOS for three different orientations of the field in a dou-

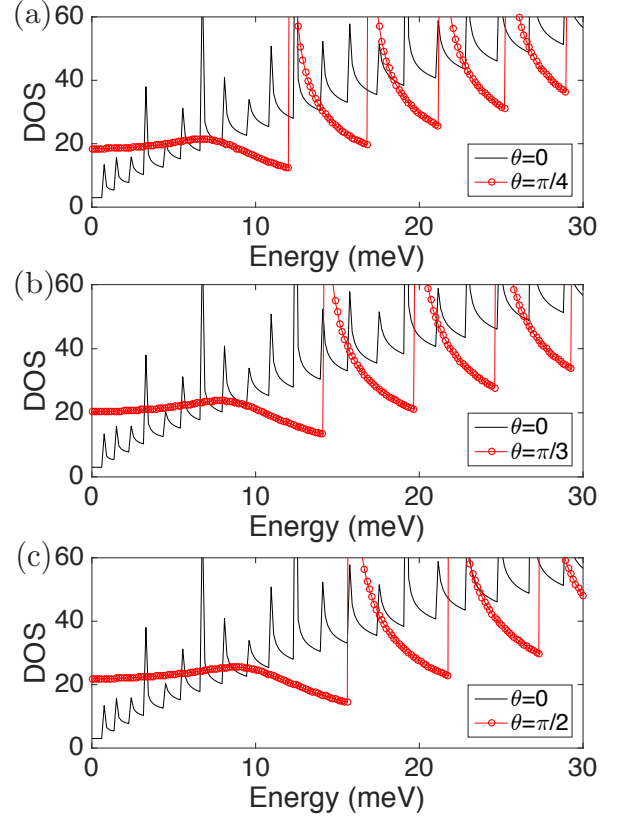


FIG. 7: (Color online) DOS for Landau levels in a triple-Weyl semimetal, in units of $L/(2\pi\hbar v_z)$. The parameters are the same as those in Fig. 5(b). The black curves are the DOS when the applied magnetic field is along the z direction ($\theta = 0$), see Eq. (16).

ble WSM. We find that the LL spacing continues to increase when the field is gradually tilted from 0 to $\pi/2$. We also notice that as $\theta \rightarrow \pi/2$ an additional peak in DOS gradually develops within the manifold of ZLLs, which, however, can be an artifact of continuum model. A similar result also holds for triple WSM, as shown in Fig. 7.

The DOS dictates the pattern of quantum oscillation measurements (through Shubnikov-de Haas effect or De Haas-van Alphen effect) of all transport and thermodynamic quantities. Therefore, the proposed anisotropic structure in DOS for multi-WSM can be detected from angle resolved quantum oscillations [40, 41]. Such experiments can also test the robustness of the emergent peak in DOS within the ZLL of double WSM by tilting the magnetic field from the z direction toward the xy plane.

V. LONGITUDINAL MAGNETOTRANSPORT

As shown in Sec. III, in the presence of strong magnetic fields the quasiparticle spectrum in any WSMs breaks

into a set of LLs that remains dispersive along the direction of the applied field. Therefore, the application of an external magnetic field effectively breaks the system into a set of one-dimensional conducting wires, which is responsible for LMT. For the sake of simplicity and specificity we assume that the external magnetic and electric (\mathbf{E}) fields are always parallel to each other (see Fig. 2). When \mathbf{B} and \mathbf{E} are not parallel, the transport occurs through both longitudinal and transverse components. However, the analysis of the transport properties for an arbitrary relative orientation of \mathbf{B} and \mathbf{E} fields falls outside the scope of the current work. To sustain a steady-state current, we take into account impurity-induced backscattering between the magnetic field induced emergent one dimensional Weyl nodes, while the forward scattering contributes to the *Dingle factor* for quantum oscillations. When such scattering is accounted for, the LMC (intra-band) can be written as

$$\sigma(B) = \sum_{\alpha} g_{\alpha} \frac{e^2 v_{F,\alpha}(B) \tau_{\alpha}(B)}{2\pi^2 \hbar \ell^2}, \quad (17)$$

where the sum is over all partially filled Landau levels labeled by α , g_{α} is the additional degeneracy due to internal degrees of freedom (such as spin), $v_{F,\alpha}(B)$ is the field dependent Fermi velocity obtained by linearizing the LL spectrum around the emergent one-dimensional Weyl nodes, and $\tau_{\alpha}(B)$ is the transport lifetime (obtained from backscattering). We here use the linearized Boltzmann equation to compute the lifetime and numerically extract the effective field dependent Fermi velocity. We assume that only the subspace of ZLLs is partially filled and contributes to LMT. Generalization of our results is discussed in Sec. V E. Two sources of elastic scattering are taken into account: (i) Gaussian disorder with

$$U^{(G)}(\mathbf{q}_{\perp}, q_z) = U_0 e^{-R_0^2(q_{\perp}^2 + q_z^2)/2}, \quad (18)$$

where R_0 is the range of the impurity potential, and (ii) long-range ionic impurity scattering characterized by the screened Coulomb potential

$$U^{(C)}(\mathbf{q}_{\perp}, q_z) = \frac{U_c}{q_{\perp}^2 + q_z^2 + q_{TF}^2}, \quad (19)$$

where $U_c \simeq 4\pi e^2/\kappa$ is the strength of the Coulomb impurity, and q_{TF} is the Thomas-Fermi wave vector q_{TF} ,

$$q_{TF}(B) = \frac{e}{\sqrt{2\pi^2 \hbar v_F(B) \ell_B^2}}, \quad (20)$$

which is also a function of the magnetic field. Therefore with an increasing magnetic field, the screened Coulomb impurity potential gets more and more short-ranged as q_{TF} increases. Hence, in the strong field limit, the LMT is dominated by Gaussian impurities. The increase in screening with increasing magnetic field follow from the enhancement of the DOS by the magnetic field. Note that in the extremely strong field limit the screened Coulomb potential becomes very small as q_{TF} diverges. Also, we find that typically the relaxation time due to Gaussian impurities is much smaller than that due to Coulomb impurities. Therefore, transport lifetime is dominated by the former source of elastic scattering.

A. Linearized Boltzmann equation

The transport lifetime $\tau_{\alpha}(B)$ can be obtained from the linearized Boltzmann equation, which reads as [85]

$$1 = \sum_{\beta, k'_y, k'_z} W(k_y, k_z, \alpha; k'_y, k'_z, \beta) \left[\tau_{\alpha}(k_z) - \frac{v_{\beta}(k'_z)}{v_{\alpha}(k_z)} \tau_{\beta}(k'_z) \right],$$

where the impurity matrix element squared is given by

$$W(k_y, k_z, \alpha; k'_y, k'_z, \beta) = \frac{2\pi n_i}{\hbar} \int \frac{d^3 q}{(2\pi)^3} |U(\mathbf{q})|^2 \times |\langle k_y, k_z, \alpha | e^{i\mathbf{q} \cdot \mathbf{r}} | k'_y, k'_z, \beta \rangle|^2 \delta[\epsilon_{\alpha}(k_z) - \epsilon_{\beta}(k'_z)]. \quad (21)$$

After some involved algebra, the linearized Boltzmann equation can be cast in the following compact form

$$\begin{aligned} \frac{\hbar^2}{n_i \ell_B^2} = & \tau_{\alpha}(k_{F,\alpha}) \left[\frac{2|U_{\alpha,\alpha}(2k_{F,\alpha})|^2}{|v_{\alpha}(k_{F,\alpha})|} + \sum_{\beta \neq \alpha} \frac{|U_{\alpha,\beta}(k_{F,\alpha} + k_{F,\beta})|^2 + |U_{\alpha,\beta}(k_{F,\alpha} - k_{F,\beta})|^2}{|v_{\beta}(k_{F,\beta})|} \right] \\ & + \sum_{\beta \neq \alpha} \frac{\tau_{\beta}(k_{F,\beta})}{|v_{\alpha}(k_{F,\alpha})|} \left[|U_{\alpha,\beta}(k_{F,\alpha} + k_{F,\beta})|^2 - |U_{\alpha,\beta}(k_{F,\alpha} - k_{F,\beta})|^2 \right], \end{aligned} \quad (22)$$

where $k_{F,\alpha} > 0$ is the magnitude of the one-dimensional Fermi momentum in Landau level α , v_{α} is the corresponding Fermi velocity and n_i is impurity density. The

effective one-dimensional interaction potential $U_{\alpha,\beta}(q_z)$

has the following form

$$|U_{\alpha,\beta}(q_z)|^2 = \int \frac{d^2 \mathbf{q}_\perp}{(2\pi)^2 \ell_B^2} |U(\mathbf{q}_\perp, q_z)|^2 |S_{\alpha,\beta}(\mathbf{q}_\perp)|^2, \quad (23)$$

where $U(\mathbf{q}_\perp, q_z)$ is the impurity potential, and $S_{\alpha,\beta}(\mathbf{q}_\perp)$ satisfies the relation

$$\begin{aligned} \langle k_y, k_z, \alpha | e^{i\mathbf{q} \cdot \mathbf{r}} | k'_y, k'_z, \beta \rangle \\ \equiv S_{\alpha,\beta}(\mathbf{q}_\perp) \delta(k_y - k'_y + q_y) \delta(k_z - k'_z + q_z). \end{aligned} \quad (24)$$

One can then solve the coupled equations in Eq. (22) and obtain the transport lifetime τ_α for each LL contributing to LMC.

We can obtain the analytical expression for effective one-dimensional potentials from Eq. (23), when the field is applied along the z direction (along which the Weyl nodes are separated in the absence of magnetic field). Let us first consider only the Gaussian impurity potential, for which the effective one-dimensional potential in a single WSM is given by

$$|U_{0,0}^{(G)}(q_z)|^2 = \frac{U_0^2 e^{-R_0^2 q_z^2}}{2\pi \ell_B^4} \frac{1}{1 + 2\lambda}, \quad (25)$$

where $\lambda = R_0^2/\ell_B^2$. However, with additional branches within the subspace of ZLLs, such as in double WSMs, supporting two ZLLs, there are the following two additional components for the effective potential

$$|U_{1,1}^{(G)}(q_z)|^2 = \frac{U_0^2 e^{-R_0^2 q_z^2}}{2\pi \ell_B^4} \frac{4\lambda^2 + 1}{(2\lambda + 1)^3}, \quad (26)$$

$$|U_{0,1}^{(G)}(q_z)|^2 = \frac{U_0^2 e^{-R_0^2 q_z^2}}{2\pi \ell_B^4} \frac{1}{(2\lambda + 1)^2}, \quad (27)$$

which respectively describes scattering potential within the $N = 1$ ZLL and that between $N = 0$ and $N = 1$ ZLLs. The above formalism can immediately be generalized for triple WSMs, supporting three copies of ZLL.

Similarly the effective one-dimensional potential arising from Coulomb impurities is given by

$$|U_{\alpha,\beta}^{(C)}(q_z)|^2 = \frac{U_c^2}{2\pi} \int_0^\infty r dr \frac{|S_{\alpha,\beta}(r)|^2}{(r^2 + \eta^2)^2}, \quad (28)$$

where $\eta^2 = Q^2 \ell_B^2 \equiv (q_z^2 + q_{\text{TF}}^2) \ell_B^2$. In single WSM

$$|U_{0,0}^{(C)}(z)|^2 = \frac{U_c^2}{8\pi} e^y \Gamma(-1, y), \quad (29)$$

where $y = \eta^2/2$ and $\Gamma(s, z)$ is the *upper incomplete Gamma function*. For double WSMs, the two additional components of the one-dimensional potential are

$$\begin{aligned} |U_{1,1}^{(C)}(q_z)|^2 &= \frac{U_c^2}{8\pi} [e^y (y + 1)(y + 3) \Gamma(-1, y) - (1 + 2y^{-1})], \\ |U_{0,1}^{(C)}(q_z)|^2 &= \frac{U_c^2}{8\pi} [-e^y (y + 1) \Gamma(-1, y) + y^{-1}], \end{aligned} \quad (30)$$

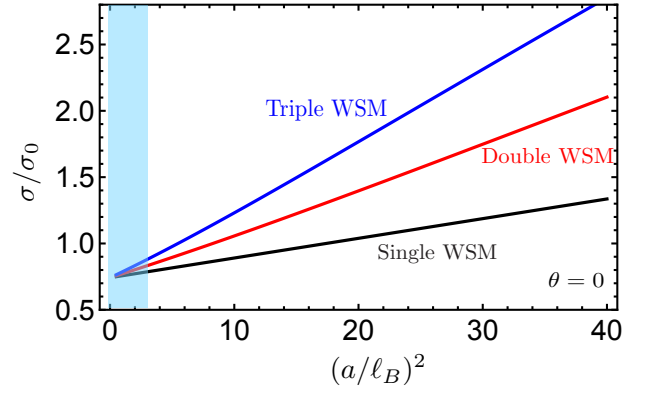


FIG. 8: A comparative plot of longitudinal magnetoconductivity (LMC) in single (black), double (red) and triple (blue) Weyl semimetals in the presence of only Gaussian impurities. The field is applied along the axis separating the Weyl nodes in pristine system (the z direction). In the shaded region Landau level are not sharp and one needs to account for weak localization effects. In this region the semiclassical theory for magnetotransport may also be applicable. Here, $\sigma_0 = e^2 \hbar v_z^2 / (2\pi n_i U_0^2)$, and for discussion see Eq. (31).

where the subscript notations are the same as that for Gaussian impurities. Note that in the extreme strong field limit, i.e., $y \rightarrow \infty$, all three effective potentials have an identical asymptotic form $|U_{0,0}^{(C)}(q_z)|^2 = |U_{0,1}^{(C)}(q_z)|^2 = |U_{1,1}^{(C)}(q_z)|^2 \simeq U_c^2 / (8\pi y^2)$. For an arbitrary orientation of the magnetic field, we extract the effective one-dimensional potentials numerically. Next we discuss the LMC in single, double and triple WSM separately.

B. Magnetotransport in a single Weyl semimetal

To set the stage, we begin with the discussion of LMT in single WSM. In the presence of only Gaussian impurities, the scattering lifetime in single WSM is given by

$$\tau_G^{(S)} = \frac{2\pi \hbar^2 \ell_B^2 |v_F|}{2n_i U_0^2 I_{RR}} = \frac{\pi \hbar^2 |v_F| \ell_B^2}{n_i U_0^2} (1 + 2\lambda) e^{4\pi^2 R_0^2 / a^2},$$

and the corresponding LMC is

$$\sigma_G^{(S)} = \frac{e^2 |v_F|}{2\pi^2 \hbar \ell_B^2} \tau_G^{(S)} = \sigma_0 (1 + 2\lambda) e^{4\pi^2 t^2}, \quad (31)$$

where $\sigma_0 = e^2 \hbar v_z^2 / (2\pi n_i U_0^2)$ and $t = R_0/a$. We have used the fact that the Fermi wave vector for backscattering in a single WSM is $q_z = \pi/a$. Therefore, LMC in single WSM, subject to only Gaussian impurities, increases linearly with the magnetic field, as shown in Fig. 8 (black curve).

The scattering lifetime due to Coulomb impurities in a single WSM is given by

$$\tau_C^{(S)} = \frac{\hbar^2 |v_F|}{2n_i \ell_B^2 |U_{0,0}^{(C)}(2k_F)|^2} = \frac{\hbar^2 |v_F|}{2n_i U_c^2 \ell_B^2} \frac{8\pi e^{-y_c}}{\Gamma(-1, y_c)}, \quad (32)$$

where $y_c = [(2k_F)^2 \ell_B^2 + q_{\text{TF}}^2 \ell_B^2] / 2$. Therefore, the total scattering lifetime (τ) in the presence of both Gaussian and Coulomb impurities is given by

$$\tau^{-1} = \tau_G^{-1} + \tau_C^{-1}, \quad (33)$$

following the *Matthiessen's rule*. Thus the total LMC in a single WSM reads

$$\sigma^{(S)} = \frac{e^2 \hbar v_F^2}{2\pi n_i a^4 U_c^2} Z^2 \left[\frac{e^{y_c}}{4} \Gamma(-1, y_c) + \frac{Z^2 \mathcal{A} e^{-4\pi^2 t^2}}{(1 + 2t^2 Z)} \right]^{-1}, \quad (34)$$

where $Z = a^2 / \ell_B^2 \propto B$. Notice that in the presence of only Coulomb impurities the LMC grows as B^2 in the extremely strong field limit. However, in the strong magnetic field limit Gaussian impurities dominate the LMT (since typically $\tau_C \gg \tau_G$) and from here onward we only take into account the scattering lifetime arising from Gaussian impurities.

C. Magnetotransport in a double Weyl semimetal

For a double WSM *at half filling*, the coupled equations in Eq. (22) can be simplified since the Fermi velocities of the two ZLLs are exactly the same by symmetry. As a result the two coupled equations for the transport lifetime can be rewritten as

$$\begin{aligned} \frac{\hbar^2 |v_F|}{n_i \ell_B^2} &= \tau_R [2\mathcal{I}_{RR} + \mathcal{I}_{RL}^{(-)} + \mathcal{I}_{RL}^{(+)}] + \tau_L [\mathcal{I}_{RL}^{(+)} - \mathcal{I}_{RL}^{(-)}], \\ &= \tau_L [2\mathcal{I}_{LL} + \mathcal{I}_{LR}^{(-)} + \mathcal{I}_{LR}^{(+)}] + \tau_R [\mathcal{I}_{LR}^{(+)} - \mathcal{I}_{LR}^{(-)}], \end{aligned} \quad (35)$$

where v_F represents the same Fermi velocity for the two ZLLs, which we label R and L , as shown in Fig. 5(a). The backscattering potentials can be written as

$$\begin{aligned} \mathcal{I}_{RR} &= |U_{R,R}(2k_{F,R})|^2, \quad \mathcal{I}_{RL}^{(\pm)} = |U_{R,L}(k_{F,R} \pm k_{F,L})|^2, \\ \mathcal{I}_{LL} &= |U_{L,L}(2k_{F,L})|^2, \end{aligned} \quad (36)$$

where $U_{i,j}(x)$ is defined in Eq. (23) and by symmetry $\mathcal{I}_{LR}^{(\pm)} = \mathcal{I}_{RL}^{(\pm)}$. Therefore, one of the scattering lifetimes is

$$\begin{aligned} \tau_R &= \\ &= \frac{(\mathcal{I}_{LL} + \mathcal{I}_{RL}^{(-)}) (\hbar^2 |v_F| / n_i \ell_B^2)}{(\mathcal{I}_{RR} + \mathcal{I}_{LL}) (\mathcal{I}_{RL}^{(+)} + \mathcal{I}_{RL}^{(-)}) + 2 (\mathcal{I}_{RR} \mathcal{I}_{LL} + \mathcal{I}_{RL}^{(+)} \mathcal{I}_{RL}^{(-)})}, \end{aligned} \quad (37)$$

and τ_L is obtained after taking $L \leftrightarrow R$ in the above expression. Since the Fermi velocities of the two ZLLs are identical at half-filling, the total transport lifetime is $\tau_L + \tau_R$ and the LMC assumes the form

$$\sigma_G(B) = \frac{e^2 \hbar}{\pi n_i U_0^2} v_F^2(B) K_G(B, \theta), \quad (38)$$

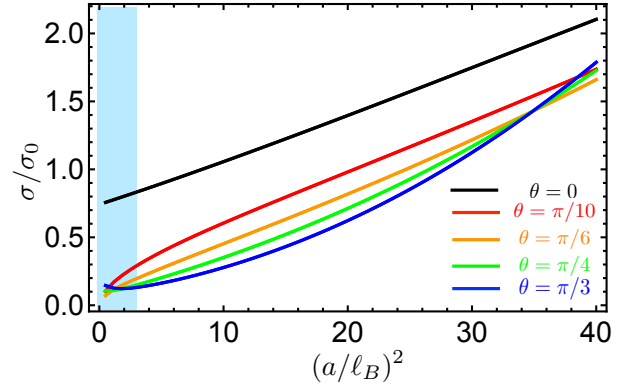


FIG. 9: A plot of longitudinal magnetoconductivity (LMC) in double Weyl semimetal for various orientations of the applied magnetic field (captured by the parameter θ). We here only account for Gaussian impurities. In the shaded region weak localization effect dominates the LMC, where our analysis is qualitatively inapplicable. Here, $\sigma_0 = e^2 \hbar v_z^2 / (2\pi n_i U_0^2)$, and for discussion see Eq. (31).

where $K_G(B, \theta)$ is a dimensionless quantity, which for $\theta = 0$ reads as

$$\begin{aligned} K_G(B, 0) &= \frac{e^{4\pi^2 t^2}}{2} \frac{(2\lambda + 1)^2 [4\lambda^2 + 2\lambda + 1 + e^{4\pi^2 t^2} (2\lambda + 1)]}{2\lambda + 4\lambda^2 (\lambda + 1) + 1 + e^{4\pi^2 t^2} (1 + 2\lambda + 2\lambda^2)}, \\ &\simeq \frac{e^{4\pi^2 t^2}}{2} \begin{cases} 1 + 4\lambda & \lambda \ll 1, \\ 2 + 4\lambda & \lambda \gg 1. \end{cases} \end{aligned} \quad (39)$$

We display $\sigma_G(B)$ for $\theta = 0$ in Fig. 8 (red curve). Thus for zero-range ($R_0 = 0$) impurities the LMC is constant, whereas for Gaussian impurities it increases monotonically and linearly with magnetic field B , thus giving rise to *positive* LMC. Also notice that in the limit $t \gg 1$ (corresponding to fat Gaussian impurities) or $\lambda \gg 1$ (corresponding to strong magnetic field) the LMC for a double WSM is exactly twice that of a single-Weyl semimetal [see Eq. (31) and Fig. 8], since the scattering between two Landau levels with different indices “L” and “R” will be suppressed in comparison to that within the same LL. Thus in the strong field limit ($\lambda \gg 1$) or fat Gaussian impurity ($t \gg 1$) limit the two ZLLs become effectively decoupled and conduct independently.

For general orientations of the magnetic field we cannot obtain the LMC analytically and we have to pursue a numerical approach. The results are shown in Fig. 9. It is interesting to notice that when $\theta \neq 0$, LMC develops *nonlinear* dependence on the field, and only at sufficiently strong fields the B -linear LMC is recovered. Such non-trivial dependence on magnetic field and tilted angle should be experimentally observable in transport measurements. For LMC in double WSM in the presence of only Coulomb or ionic impurities see Appendix B.

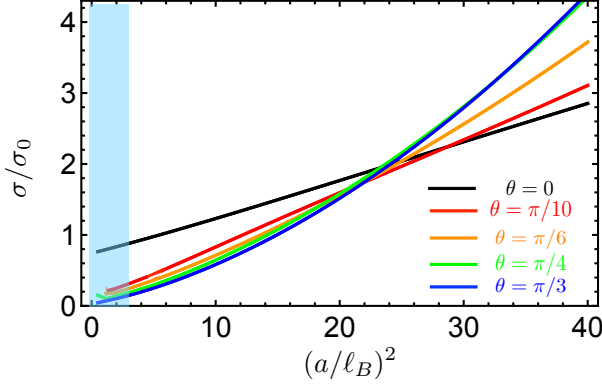


FIG. 10: A plot of longitudinal magnetoconductivity (LMC) in triple Weyl semimetal for various orientations of the applied magnetic field (captured by the parameter θ). We here only account for Gaussian impurities. In the shaded region weak localization effect dominates the LMC, where our analysis is qualitatively inapplicable. Here, $\sigma_0 = e^2 \hbar v_z^2 / (2\pi n_i U_0^2)$, and for discussion see Eq. (31).

D. Magnetotransport in a triple Weyl semimetal

Finally we discuss LMC in triple WSM by restricting ourselves to Gaussian impurities. Unlike double WSM, the Fermi velocities of the three ZLLs (at and near half filling) are no longer equal: in general we have $v_L = v_R \neq v_C$, where “L”, “C”, and “R” are the labels for the three branches of ZLL, shown in Fig. 5(b). The LMC then assumes the following form,

$$\begin{aligned} \sigma(B) &= \frac{e^2 \hbar v_L}{\pi n_i U_0^2} [v_L(\tau_L + \tau_R) + v_C \tau_C] \\ &= \sigma_0 \left\{ \frac{v_L^2(B)}{v_z^2} [\tilde{\tau}_L + \tilde{\tau}_R + w^{-1} \tilde{\tau}_C] \right\}, \end{aligned} \quad (40)$$

where $w = v_L/v_C$ and $\tilde{\tau}_i = n_i U_0^2 \tau_i / (2\pi \ell^2 \hbar^2 v_L)$ is a dimensionless quantity.

The LMC in a triple WSM can be obtained analytically when the magnetic field is applied along the z direction ($\theta = 0$), see Fig. 8 (blue curve). Notice all three Fermi velocities are then equal ($w = 1$). For sufficiently strong magnetic fields ($\lambda \gg 1$) or fat Gaussian impurity potential ($t \gg 1$), three ZLLs again behave as decoupled one-dimensional wires and the LMC in a triple WSM is three times that of a single WSM; compare black and blue curves in Fig. 8.

For arbitrary orientations of the magnetic field, we compute various scattering elements, shown in Eq. (40), numerically. In particular, notice that three Fermi vectors for backscattering have the magnitudes of π/a , and $\pi/a \pm k_c$, respectively, where k_c is again a function of the direction and strength of the applied magnetic field. The resulting LMC in triple WSM is shown in Fig. 10. Similar to the situation in double WSM, the LMC in triple WSM also exhibits an anisotropic angular dependence on the field orientations. In particular, as the tilting angle θ

increases LMC displays a smooth crossover from B -linear to *nonlinear* in B dependence, but LMC always remains positive.

E. Generic chiral anomaly and magnetotransport away from half-filling

So far we discussed the LMT in general WSMs when the system is at precisely half-filling and consequently only the subspace of ZLLs is partially filled. However, our conclusions remain qualitatively valid even when (i) the system is away from half-filling, (ii) higher LLs are also partially filled. Let us first focus on the former situation. When the system is placed away from half-filling with increasing strength of the magnetic field, as the DOS of LLs increases the chemical potential continuously shifts toward the half-filling value (since carrier density is fixed) and at infinite field limit the chemical potential gets locked at band center or zero energy. Hence, our theoretical prediction regarding the fate of LMC and its scaling with the magnetic field at half-filling is achieved for a strong enough field, but the outcomes remain qualitatively operative, as long as only the subspace of ZLLs is partially field.

When multiple LLs are partially filled (including the zeroth ones), any WSM supports positive LMC, since its origin relies on the existence of partially filled LLs. As a generic property of any three-dimensional metallic system, since for each partially filled LLs there exists at least a pair of emergent one-dimensional Weyl points (characterized by one-dimensional chiral fermions). With the emergence of such Weyl nodes our analysis of LMT remains operative and the system continues to support positive LMC. However, with increasing number of partially filled LLs, the number of backscattering channels increases rapidly and the calculation of relaxation lifetime gets involved. Nonetheless, one can borrow our analysis (at least qualitatively) for multi WSMs ($n > 1$), in particular when the field is tilted away from the z direction, for which we have established generic positive LMC. Hence, we believe that positive LMC in general WSM should be a generic situation when the system is in the quantum limit ($\omega_c \tau \gg 1$), irrespective of the location of the chemical potential.

The magnetotransport results presented in this section are valid only when the WSM remains in its normal ‘Fermi liquid’ phase, i.e., there is no symmetry-breaking transition induced by interactions. Any quantitative interaction effects can be included in the theory simply by reinterpreting each parameter as the corresponding renormalized quantity within a Fermi liquid phase. In particular, the results from this section would not apply in the presence of any field-induced density wave ordering, which might happen due of electronic interactions. Next we will discuss the effect of various density-wave ordering within the manifold of ZLLs and its effects on

LMT. Our conclusions regarding the effects of density-wave ordering on LMT can easily be generalized when the chemical potential placed deep inside the valence or conduction like LLs, so that multiple LLs (including the zeroth one) are partially filled.

VI. ELECTRONIC INTERACTION AND DENSITY-WAVE ORDERINGS

The DOS in a WSM, constituted by Weyl nodes with monopole charges $\pm n$, vanishes as $E^{2/n}$ as one approaches the Weyl points. Here the energy E is measured from the Weyl points. Therefore, any weak electron-electron interaction (restricting ourselves to Hubbard-like local interactions, as appropriate for tight-binding lattice models) is an *irrelevant* perturbation around the noninteracting Gaussian fixed point, and Weyl semimetals describe an infrared stable fixed point in the language of renormalization group. However, a strong magnetic field quenches the quasiparticle dispersion into a set of discrete LLs, all of them dispersing along the applied magnetic field. The DOS for such effective one-dimensional systems is *constant*, significantly enhancing the effects of electron-electron interaction. Therefore, sufficiently strong magnetic fields can hybridize the emergent Weyl nodes and gap them out through the formation of a density-wave order that breaks the *translational symmetry*. Such a mechanism of developing density-wave order remains operative in any three-dimensional interacting electronic system in the presence of a strong external magnetic field [92, 94–96]. In the continuum limit the CDW or SDW order breaks an emergent *continuous* $U(1)$ translational symmetry [92, 97–99], and disorder can couple to density-wave order as *random field*. The Imry-Ma argument then prohibits such an order from acquiring a true long-range order [89]. However, in the presence of an underlying lattice, the density-wave orders only break *discrete* translational symmetry. Hence, our proposed density-wave order (CDW or SDW) can exhibit a true long range ordering and may be observable at moderately strong magnetic fields. For the sake of simplicity, we here assume that only the manifold of ZLLs are partially filled, and concomitantly, density-wave ordering develops within this manifold. The following discussion can easily be generalized when multiple LLs are partially filled, but the quantitative details will be different with the density wave ordering trend being suppressed as more LLs participate in the energetics. In addition, the actual nature of the density-wave ordering (CDW or SDW) within ZLLs depends on the microscopic details of the Weyl system, as we discuss below.

To capture the low energy physics in such WSMs we appropriately define a four component spinor as $\Psi^\top(\vec{k}) = [\Psi_L(\vec{k}), \Psi_R(\vec{k})]$, where $\Psi_X(\vec{k})$ are two component spinors for left (L) and right (R) chiral fermions, organized as $\Psi_X^\top(\vec{k}) = [\Psi_{X,\uparrow}(\pm\vec{Q} + \vec{k}), \Psi_{X,\downarrow}(\pm\vec{Q} + \vec{k})]$ for $X = L, R$.

In this notation, Weyl nodes are located at $\pm\vec{Q}$ and \uparrow, \downarrow are the Kramers partners or two spin projections. Let us first focus on the low energy Hamiltonian for WSMs, shown in Eq. (7), which can be written compactly as

$$H_{0,n} = \tau_0 \otimes [\sigma_1 \cos \theta_k + \sigma_2 \sin \theta_k] \alpha_n k_\perp^n + \tau_3 \otimes \sigma_3 v_z k_z, \quad (41)$$

where $\theta_k = \tan^{-1}(k_y/k_x)$. For such Weyl systems $\vec{Q} = Q\hat{z}$, hence the Weyl nodes are along the z direction. Notice that two distinct types of density-wave orders, namely the CDW and SDW, can gap out the Weyl nodes at the cost of the translational symmetry. Respectively the effective single-particle Hamiltonian in the presence of these two orderings are

$$H_{C/S} = \Delta_{C/S} (\tau_1 \otimes \cos \phi + \tau_2 \otimes \sin \phi) \otimes \sigma_0. \quad (42)$$

In the continuum description ϕ is a continuous variable, and these two ordered phases break continuous $U(1)$ chiral symmetry generated by $U_c = \tau_3 \otimes \sigma_0$, representing the generator of translational symmetry [92], and $[H_{0,n}, U_c] = 0$, whereas $\{U_c, H_x\} = 0$ for $x = C$ and S . But, the underlying lattice potential lifts such continuous symmetry and prefers certain locking angle for the order parameter. Therefore, the ordered phase is not accompanied by true massless Goldstone mode, similar to the situation with underlying valence bond solid or superconductor in two-dimensional graphene [100].

Even though both CDW and SDW orders gap out the ZLLs, a subtle competition between these two orders may ultimately determine the actual pattern of the symmetry breaking. Notice that $\{H_{0,n}, H_S\} = 0$ and the SDW order stands as a chiral symmetry breaking *mass* for Weyl fermions. Thus, when SDW order sets in, besides gapping out the ZLLs, it also pushes down all filled LLs, following the spirit of *magnetic catalysis* [101, 102]. Hence, the SDW order appears to be energetically favored over CDW, when Weyl nodes are located along one of the C_{4v} axes of a cubic system, for example k_z .

It is also conceivable to realize the Weyl semimetals for which the low energy Hamiltonian is given by

$$H_{0,n} = \tau_3 \otimes [\alpha_n k_\perp^n [\sigma_1 \cos \theta_k + \sigma_2 \sin \theta_k] + \sigma_3 v_z k_z], \quad (43)$$

when the Weyl nodes are located along (1,1,1) direction in a cubic system, for example, and $\vec{Q} = Q(1,1,1)/\sqrt{3}$. Once again both CDW and SDW orders can generate a spectral gap within the manifold of ZLLs. However, the role of the CDW and SDW orders is now reversed; CDW representing a chiral symmetry breaking mass. Hence, in a WSM for which the Weyl nodes are placed along one of the C_{3v} axes of a cubic system and the low energy Hamiltonian assumes the form in Eq. (43), the CDW order is energetically favored over the SDW one. Thus the nature of the density-wave ordering crucially depends on the microscopic details of the system. However, the signature of such translation symmetry breaking ordering on LMT is qualitatively insensitive to its actual nature since in both cases spectral gaps open up within the ZLLs.

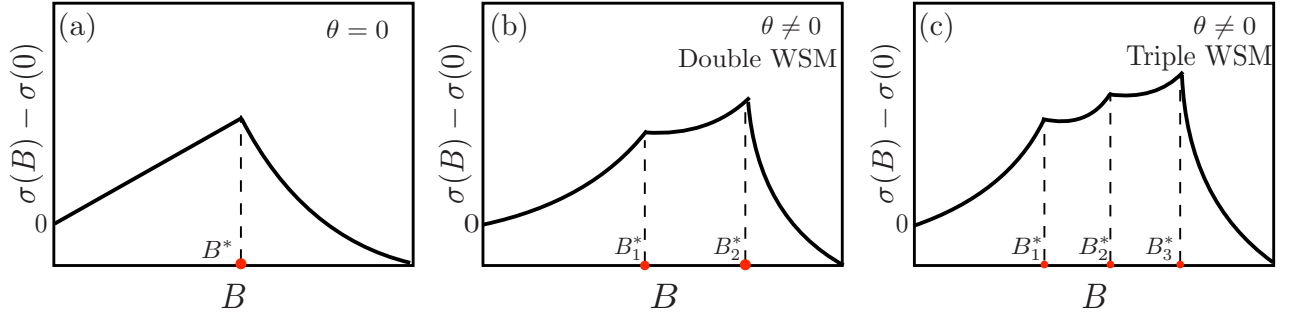


FIG. 11: A schematic variation of longitudinal magnetoconductivity (LMC) upon accounting for density-wave instabilities (either CDW or SDW) within the subspace of the zeroth Landau levels (ZLLs). (a) Qualitative variation of LMC is shown for any WSMs (constituted by Weyl nodes with monopole charge n) when the field is applied along the z direction, and therefore n number of ZLLs are exactly degenerate in a WSM. LMC becomes positive when $B > B^*$. Qualitative variation of LMC in (b) double and (c) triple Weyl semimetals when the field is tilted away from the z direction (assuming the Weyl nodes are separated along the z direction in the absence of magnetic field). Separate discontinuities in LMC arise since the n ZLLs are no longer degenerate when $\theta \neq 0$. Each discontinuity is associated with the density-wave ordering in separate branches of the ZLLs, before LMC become negative when all ZLLs are gapped out.

As shown in the previous section, due to partially filled subspace of ZLLs, all WSMs manifest positive LMC or negative LMR, when these systems are placed in a strong magnetic field. On the other hand, electronic interaction can be conducive for translational symmetry breaking CDW or SDW order that produces a spectral gap within the ZLL. With the onset of such insulating ordering there is no partially filled LL in the system and LMR (LMC) can now display an upturn (downturn) and become positive (negative) in a strong magnetic field. Although such an instability occurs for an infinitesimal strength of interaction in a clean system for $T < T_c$, with T_c being the transition temperature that scales as $T_c \sim \exp[-1/(gD(B))]$, where g is the strength of interaction responsible for density-wave ordering and $D(B)$ is the DOS of ZLLs (following the BCS scaling law), the presence of disorder may hinder its onset. This can be seen most easily by realizing that the DOS $D(B)$ is suppressed by impurity scattering (e.g. Dingle temperature effect) leading to a strong suppression of T_c [95]. Thus only for sufficiently strong magnetic fields and at low temperature these orderings can set in and the system can display an upturn in LMR. When the magnetic field is applied along z direction, all ZLLs are degenerate in double and triple WSM (in a single WSM there is always only one ZLL); hence they simultaneously undergo manybody instability toward the formation of a density-wave order as temperature is gradually lowered below T_c . Concomitantly, all WSMs display negative LMC or positive LMR above a unique strength of magnetic field $B > B_*$, when the field is applied along the z direction. The periodicity of such density-wave ordering is $2 \times \pi/(2a)$. However, the situation changes dramatically when the field is tilted away from the z direction in double and triple WSMs.

As shown in Sec. III, when the magnetic field is tilted away from the z direction, the exact degeneracy among

the ZLLs in double and triple WSM is lifted. As a result, the density-wave ordering in each ZLL is characterized by different transition temperatures, even though the degeneracy of the ZLL does not change with the field orientation, which can be qualitatively understood in the following way. For the sake of simplicity we can assume that short-range interactions arise from its long range Coulomb tail, which in three spatial dimensions scales as $V(q) \sim q^{-2}$. Then it is natural to assume that electronic interaction is stronger for density-wave ordering with smaller wave vectors since $V(q)$ increases for smaller q . Therefore, in double WSMs, as the temperature (magnetic field) is gradually lowered (increased) the Fermi points marked by “R” get gapped out first, followed by the ones marked by “L” [see Fig. 5(a)]. The periodicity of density-wave ordering in the “R” and “L” channels is respectively $2[\pi/2 \pm \delta(\theta)]/a$ where $\delta(\theta)$ depends on the orientation of the magnetic field. Similarly, in triple WSM, the mass generation first takes place among the “R” points, followed by the “C” points and finally the “L” points, see Fig. 5(b). The periodicity of density-wave ordering in these three channels are $2[\pi/2 + j\delta(\theta)]/a$, for $j = -1, 0, 1$ respectively for “R”, “C” and “L” channels. Thus as the temperature is gradually lowered in double and triple WSMs (with field tilted away from the z direction), they undergo a cascade of transitions into density-wave phases with different periodicity, and below each such transition temperature the LMC displays *discontinuity* and its rate of growth decreases, before it becomes negative when all ZLLs are gapped out, as shown in Fig. 11 (b) and (c). In other words, in single WSM the LMR becomes positive once the density-wave ordering sets in, while in double (triple) Weyl semimetal LMR should display a two (three) stage transition toward a positive value. The separation among the transition temperature or onset magnetic field (B_j^*) among various density-wave transitions (hence the distance among

various discontinuities in LMC/LMR) gets bigger as the magnetic field is gradually tilted away from the z direction, since the emergent one-dimensional Fermi points gets further separated with increasing tilting of the magnetic field away from the axis separating two Weyl nodes [see Figs. 5(a), 5(b)]. Such steps in LMR can possibly be detected in experiments and may serve as an indication for density-wave ordering in the system. As a final remark, we would like to point out that recent magneto-transport measurements in graphite (for band structure see Refs. [103, 104]) is strongly suggestive of a density-wave ordering in strong magnetic fields [105].

VII. SUMMARY AND DISCUSSION

To summarize, we here address several important aspects of Weyl semimetals when these systems are placed in a strong magnetic field. In the absence of magnetic fields, three-dimensional Weyl semimetals are constituted by Weyl nodes that can be classified according to the monopole charge $n = 1, 2$ and 3 . The integer monopole charge (n) determines the topological invariant of a Weyl semimetal, and the surface Fermi arc in such systems possesses an additional n -fold *orbital* degeneracy. When placed in a magnetic field, the underlying topological invariant manifests itself through the number of chiral zeroth Landau levels. Thus double and triple Weyl semimetals respectively support two and three copies of the zeroth Landau level while a regular or single Weyl semimetal is devoid of any flavor degeneracy when the magnetic field is applied in the z direction, along which the Weyl nodes are separated in the momentum space. The same conclusion also follows from a calculation based on a lattice model, as shown in Appendix A. Within the framework of the continuum description of these system, we always find n zeroth Landau levels, irrespective of the direction of the applied magnetic field, although their exact degeneracy breaks down when the field is tilted away from the z direction. Also the density of states in the presence of Landau levels displays a strong angular dependence, which can be observed in angle resolved quantum oscillation experiments.

We also show that the formation of Landau levels in Weyl materials can generically lead to longitudinal magnetotransport, since they are dispersive in the direction of the applied magnetic field. To obtain a steady state magnetoconductivity we invoke the relaxation mechanism arising from the backscattering by impurities and take into account two sources of elastic scattering (a) Gaussian impurity and (b) Coulomb impurity. However, due to finite density of states, the scattering potential in the effective one-dimensional world is always short ranged, and we mainly focus on the former source of elastic scattering since the Coulomb disorder is strongly screened by the carriers. Assuming that (i) the system is in the quantum limit ($\omega_c\tau > 1$), and (ii) only the sub-

space of zeroth Landau level is partially filled, we calculate the magnetic field dependence of transport lifetime in the presence of strong backscattering using the quantum Boltzmann equation and show that the longitudinal magnetoconductivity increases linearly with the applied magnetic field, when the field is applied along the separation of Weyl nodes in the pristine system. Within the low-energy approximation, we find that such linear- B dependence of the longitudinal magnetoconductance in double and triple Weyl semimetals smoothly crosses over to a nonlinear B dependence when the field is tilted away from the z direction, which can be tested experimentally. The longitudinal magnetoconductivity in all Weyl semimetals scales as B^2 when the magnetic field is applied along the separation of two pristine Weyl nodes, in the presence of Coulomb/ionic impurities, but in the extremely strong field limit.

In order to verify our predictions of LMC in systems dominant by Gaussian (short-ranged) and Coulomb (long-ranged) impurities, as well as the crossover between them, one can systematically introduce short-ranged or long-ranged impurities in a given sample, and vary their concentrations in a controlled way. For example, long-range disordered potentials can be generated by dopant charged impurities, while short-range disordered potentials can be introduced by radiation damage. Such an experimental technique provided the key evidence in finding out the relative importance of long-range versus short-range disorder potentials in the transport properties of graphene [106]. Therefore, a similar technique could in principle be used in WSMs to test our predictions with respect to longitudinal magnetotransport.

Finally, we also address the effects of electron-electron interaction on longitudinal magnetotransport in Weyl semimetals. Due to the finite density of states of effective one-dimensional system, Weyl fermions are susceptible to various types of translational symmetry breaking density-wave ordering (charge or spin depending on microscopic details) even for infinitesimal strength of interaction in the presence of strong external magnetic fields. Since a single Weyl semimetal hosts one zeroth Landau level, the onset of a density wave order immediately gives rise to positive longitudinal magnetoresistance. Such upturn in LMR can be observed below the transition temperature for sufficiently strong magnetic fields. A similar situation arises in double and triple Weyl semimetals when the field is applied along the z direction, since all zeroth Landau levels are exactly degenerate. However, the situation changes dramatically as the applied field is gradually tilted away from the z direction. Since, the two/three zeroth Landau levels in double/triple Weyl semimetals are no longer degenerate, they respectively undergo two and three transitions into density-wave phases, characterized by different periodicity as well as transition temperature. Thus, as the temperature is gradually lowered in the presence of a strong magnetic field (applied at a finite angle with respect to the z direction), the decrease of the longitudinal magnetoresistance with magnetic field

gets slower across each such transition, before it finally becomes positive when all members of the zeroth Landau level are gapped out by density-wave orderings. Thus future experiments in various members of Weyl semimetals, when placed in a magnetic field, can display intriguing confluence of Landau quantization, longitudinal magnetotransport (possibly manifesting one-dimensional chiral or axial anomaly), and interaction driven charge/spin-density-wave ordering.

Acknowledgments

This work was supported by JQI-NSF-PFC and LPS-MPO-CMTC. We thank Pallab Goswami, M. Zahid Hasan for discussion. B. R. is thankful to Nordita, Center for Quantum Materials for hospitality where part of this work was finalized.

Appendix A: Landau levels in a general Weyl semimetal from a tight-binding model

In this appendix we show the derivation of LL spectrum for single, double and triple WSM from a lattice model (bounded dispersion), when the magnetic field is applied along the separation of Weyl nodes, i.e. along the z direction. Let us begin with the following model for a general WSM

$$H = \left[t_z \cos(k_z) - m_z + \frac{\hbar^2 k_x^2 + \hbar^2 k_y^2}{2m} \right] \sigma_z + \begin{pmatrix} 0 & \alpha_n(\hbar k_x - i\hbar k_y)^n \\ \alpha_n(\hbar k_x + i\hbar k_y)^n & 0 \end{pmatrix}, \quad (\text{A1})$$

where n is the monopole charge. If the applied magnetic field is along the z direction, the Landau level spectrum of this model can be expressed in a closed form. For example, for a single WSM ($n = 1$) we have for $N \geq 1$

$$E = \pm \sqrt{\left[\epsilon_z + \frac{\hbar^2}{2m\ell_B^2}(2N+1) \right]^2 + \frac{2\alpha_1^2 \hbar^2}{\ell_B^2} N}, \quad (\text{A2})$$

where $\epsilon_z = t_z \cos(k_z) - m_z$, and N is the Landau level index. The energy dispersion for double ($n = 2$) and triple ($n = 3$) WSM can be similarly obtained as follows,

$$\begin{aligned} E_{N,m}(k_z) & \quad (\text{A3}) \\ &= \pm \left[\left[\epsilon_z + \frac{\hbar^2}{2m\ell_B^2}(2N+1) \right]^2 + \frac{4\hbar^4 \alpha_2^2}{\ell^4} N(N-1) \right]^{\frac{1}{2}}, \\ &= \pm \left[\left[\epsilon_z + \frac{\hbar^2}{2m\ell_B^2}(2N+1) \right]^2 + \frac{8\hbar^6 \alpha_3^2}{\ell^6} N(N-1)(N-2) \right]^{\frac{1}{2}} \end{aligned}$$

which is valid for $N \geq 2$ and $N \geq 3$, respectively. The resulting LL spectrum for single WSM has already been

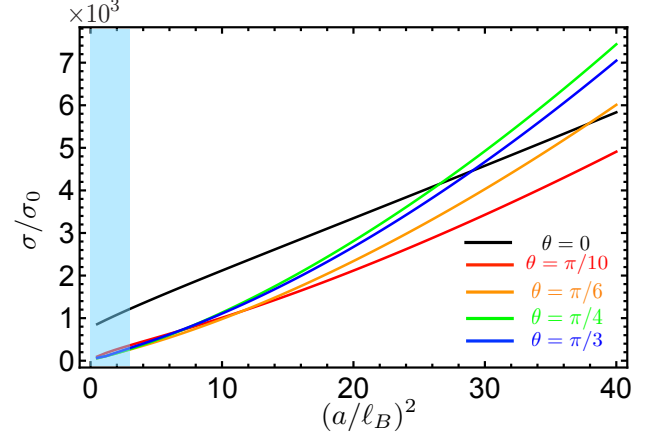


FIG. 12: A plot of longitudinal magnetoconductivity (LMC) in double Weyl semimetal for various orientations of the applied magnetic field (captured by the parameter θ). We here only account for Coulomb impurities. In the shaded region weak localization effect dominates the LMC, where our analysis is qualitatively inapplicable.

displayed in Fig. 4. The energy of the ZLL (respectively one, two and three fold degenerate in single, double and triple WSM) is

$$E_0(k_z) = t_z \cos(k_z) - m_z + \frac{\hbar^2}{2m\ell_B^2} \quad (\text{A4})$$

and throughout we measured the energy from the reference value or zero point energy $\hbar^2/(2m\ell_B^2)$.

Appendix B: Magnetoconductivity by Coulomb impurities

In this appendix we want to briefly discuss the LMC in double WSMs only in the presence of Coulomb impurities. The results are displayed in Fig. 12 for various field orientations. We note that typically the transport lifetime due to Coulomb impurities are much longer than that for Gaussian impurities. Thus according to the Matthiessen's rule, shown in Eq. (33), the transport lifetime is dominated by Gaussian impurities. However, in the complete absence of Gaussian impurities, one can expect to observe the LMC shown in Fig. 12. We also want to note that LMC driven by Coulomb impurities will show a B^2 dependence only in the limit of $B \rightarrow \infty$. We also find similar field dependence of LMC in the presence of only Coulomb impurities in single as well as triple WSMs.

- [1] M. Z. Hasan, and C. L. Kane, *Colloquium: Topological insulators*, Rev. Mod. Phys. **82**, 3045 (2010).
- [2] X-L. Qi, and S-C. Zhang, *Topological insulators and superconductors*, Rev. Mod. Phys. **83**, 1057 (2011).
- [3] J. D. Sau, R. M. Lutchyn, S. Tewari, and S. Das Sarma *Generic New Platform for Topological Quantum Computation Using Semiconductor Heterostructures*, Phys. Rev. Lett. **104**, 040502 (2010).
- [4] L. Fu and Y. Ando, *Topological Crystalline Insulators and Topological Superconductors: From Concepts to Materials*, Annu. Rev. Condens. Matter Phys. **6**, 361 (2015).
- [5] M. Dzero, J. Xia, V. Galitski, and P. Coleman, *Topological Kondo Insulators*, Annu. Rev. Condens. Matter Phys. **7**, 249 (2016).
- [6] M. Z. Hasan, S.-Y. Xu, and M. Neupane, *Topological Insulators, Topological Crystalline Insulators, Topological Semimetals and Topological Kondo Insulators*, arXiv:1406.1040 (2014).
- [7] G. E. Volovik, *The Universe in a Helium Droplet* (Oxford University Press, New York, 2003).
- [8] A. A. Burkov, *Chiral anomaly and transport in Weyl metals*, J. Phys.: Condens. Matter **27**, 113201 (2015).
- [9] S. Rao, *Weyl semi-metals : a short review*, arXiv:1603.02821 (2016).
- [10] H. Weng, C. Fang, Z. Fang, A. Bernevig, X. Dai, *Weyl semimetal phase in non-centrosymmetric transition metal monophosphides*, arXiv:1501.00060 (2015).
- [11] S.-M. Huang, S.-Y. Xu, I. Belopolski, C.-C. Lee, G. Chang, B. Wang, N. Alidoust, G. Bian, M. Neupane, A. Bansil, H. Lin, and M. Z. Hasan, *An inversion breaking Weyl semimetal state in the TaAs material class*, arXiv:1501.00755 (2015).
- [12] S.-Y. Xu, I. Belopolski, N. Alidoust, M. Neupane, C. Zhang, R. Sankar, S.-M. Huang, C.-C. Lee, G. Chang, B. Wang, G. Bian, H. Zheng, D. S. Sanchez, F. Chou, H. Lin, S. Jia, and M. Z. Hasan, *Experimental realization of a topological Weyl semimetal phase with Fermi arc surface states in TaAs*, arXiv:1502.03807 (2015).
- [13] C. Zhang, Z. Yuan, S.-Y. Xu, Z. Lin, B. Tong, M. Z. Hasan, J. Wang, C. Zhang, and S. Jia, *Tantalum Monoarsenide: an Exotic Compensated Semimetal*, arXiv:1502.00251 (2015).
- [14] S.-Y. Xu, I. Belopolski, N. Alidoust, M. Neupane, G. Bian, C. Zhang, R. Sankar, G. Chang, Z. Yuan, C.-C. Lee, S.-M. Huang, H. Zheng, J. Ma, D. S. Sanchez, B. Wang, A. Bansil, F. Chou, P. P. Shibayev, H. Lin, S. Jia, and M. Z. Hasan, *Discovery of a Weyl fermion semimetal and topological Fermi arcs*, Science **349**, 613 (2015).
- [15] B. Q. Lv, H. M. Weng, B. B. Fu, X. P. Wang, H. Miao, J. Ma, P. Richard, X. C. Huang, L. X. Zhao, G. F. Chen, Z. Fang, X. Dai, T. Qian, and H. Ding, *Experimental Discovery of Weyl Semimetal TaAs*, Phys. Rev. X **5**, 031013 (2015).
- [16] S.-Y. Xu, N. Alidoust, I. Belopolski, Z. Yuan, G. Bian, T.-R. Chang, H. Zheng, V. N. Strocov, D. S. Sanchez, G. Chang, C. Zhang, D. Mou, Y. Wu, L. Huang, C.-C. Lee, S.-M. Huang, B. Wang, A. Bansil, H.-T. Jeng, T. Neupert, A. Kaminski, H. Lin, S. Jia, and M. Zahid Hasan, *Discovery of a Weyl fermion state with Fermi arcs in niobium arsenide*, Nat. Phys. **11**, 748 (2015).
- [17] N. Xu, H. M. Weng, B. Q. Lv, C. Matt, J. Park, F. Bisti, V. N. Strocov, D. Gawryluk, E. Pomjakushina, K. Conder, N. C. Plumb, M. Radovic, G. Auts, O. V. Yazyev, Z. Fang, X. Dai, G. Aeppli, T. Qian, J. Mesot, H. Ding, M. Shi, *Observation of Weyl nodes and Fermi arcs in TaP*, arXiv:1507.03983 (2015).
- [18] H. Inoue, A. Gyenis, Z. Wang, J. Li, S. W. Oh, S. Jiang, N. Ni, B. A. Bernevig, A. Yazdani, *Quasiparticle interference of the Fermi arcs and surface-bulk connectivity of a Weyl semimetal*, Science **351**, 1184 (2016).
- [19] S. Kourtis, J. Li, Z. Wang, A. Yazdani, B. A. Bernevig, *Universal signatures of Fermi arcs in quasiparticle interference on the surface of Weyl semimetals*, Phys. Rev. B **93**, 041109 (2016).
- [20] C. Shekhar, A. K. Nayak, Y. Sun, M. Schmidt, M. Nicklas, I. Leermakers, U. Zeitler, Z. Liu, Y. Chen, W. Schnelle, J. Grin, C. Felser, B. Yan, *Extremely large magnetoresistance and ultrahigh mobility in the topological Weyl semimetal NbP*, arXiv:1502.04361 (2015).
- [21] Z. Wang, Y. Zheng, Z. Shen, Y. Lu, H. Fang, F. Sheng, Y. Zhou, X. Yang, Y. Li, C. Feng, and Z.-A. Xu, *Helicity-protected ultrahigh mobility Weyl fermions in NbP*, Phys. Rev. B **93**, 121112 (2016).
- [22] G. Chang, S.-Y. Xu, D. S. Sanchez, S.-M. Huang, C.-C. Lee, T.-R. Chang, H. Zheng, G. Bian, I. Belopolski, N. Alidoust, H.-T. Jeng, A. Bansil, H. Lin, M. Z. Hasan, *A strongly robust Weyl fermion semimetal state in Ta₃S₂*, arXiv:1512.08781 (2015).
- [23] S. Borisenko, D. Evtushinsky, Q. Gibson, A. Yaresko, T. Kim, M. N. Ali, B. Buechner, M. Hoesch, R. J. Cava, *Time-reversal symmetry breaking Weyl state in YbMnBi₂*, arXiv:1507.04847 (2015).
- [24] J. Y. Liu, J. Hu, Q. Zhang, D. Graf, H. B. Cao, S. M. A. Radmanesh, D. J. Adams, Y. L. Zhu, G. F. Cheng, X. Liu, W. A. Phelan, J. Wei, D. A. Tennant, J. F. DiTusa, I. Chiorescu, L. Spinu, Z. Q. Mao, *Discovery of a topological semimetal phase coexisting with ferromagnetic behavior in Sr_{1-y}Mn_{1-z}Sb₂*, arXiv:1507.07978 (2015).
- [25] A. A. Burkov, and L. Balents, *Weyl Semimetal in a Topological Insulator Multilayer*, Phys. Rev. Lett. **107**, 127205 (2011).
- [26] A. A. Burkov, M. D. Hook, and L. Balents, *Topological nodal semimetals*, Phys. Rev. B **84**, 235126 (2011).
- [27] A. A. Zyuzin, S. Wu, and A. A. Burkov, *Weyl semimetal with broken time reversal and inversion symmetries*, Phys. Rev. B **85**, 165110 (2012).
- [28] T. Das, *Weyl semimetal and superconductor designed in an orbital-selective superlattice*, Phys. Rev. B **88**, 035444 (2013).
- [29] Q. D. Gibson, L. M. Schoop, L. Muechler, L. S. Xie, M. Hirschberger, N. P. Ong, R. Car, and R. J. Cava, *3D Dirac semimetals: current materials, design principles and predictions of new materials*, arXiv:1411.0005 (2014).
- [30] S. Ganeshan and S. Das Sarma, *Constructing a Weyl semimetal by stacking one-dimensional topological phases*, Phys. Rev. B **91**, 125438 (2015).
- [31] X. Wan, A. Turner, A. Vishwanath, and S. Y. Savrasov, *Topological semimetal and Fermi-arc surface states in*

- the electronic structure of pyrochlore iridates, Phys. Rev. B **83**, 205101 (2011).
- [32] E.-G. Moon, C. Xu, Y. B. Kim, L. Balents, *Non-Fermi liquid and topological states with strong spin-orbit coupling*, Phys. Rev. Lett. **111**, 206401 (2013).
- [33] S. B. Lee, Y. B. Kim, and A. Paramakanti, *RKKY interactions and anomalous Hall effect in metallic rare-earth pyrochlores*, Phys. Rev. Lett. **111**, 196601 (2013).
- [34] P. Goswami, B. Roy, and S. Das Sarma, *Itinerant spin ice order, Weyl metal, and anomalous Hall effect in $Pr_2Ir_2O_7$* , arXiv:1603.02273 (2016).
- [35] C. Herring, *Effect of Time-Reversal Symmetry on Energy Bands of Crystals*, Phys. Rev. **52**, 361 (1937); *Accidental Degeneracy in the Energy Bands of Crystals*, Phys. Rev. **52**, 365 (1937).
- [36] H. B. Nielsen and M. Ninomiya, *A no-go theorem for regularizing chiral fermions*, Phys. Lett. B **105**, 219 (1981).
- [37] C. Fang, M. J. Gilbert, X. Dai, and B. A. Bernevig, *Multi-Weyl Topological Semimetals Stabilized by Point Group Symmetry*, Phys. Rev. Lett. **108**, 266802 (2012).
- [38] B.-J. Yang and N. Nagaosa, *Classification of stable three-dimensional Dirac semimetals with nontrivial topology*, Nature Communication **5**, 4898 (2014).
- [39] S.-M. Huang, S.-Y. Xu, I. Belopolski, C.-C. Lee, G. Chang, B. Wang, N. Alidoust, M. Neupane, H. Zheng, D. Sanchez, A. Bansil, G. Bian, H. Lin, M. Z. Hasan, *New type of Weyl semimetal with quadratic double Weyl fermions*, PNAS **113**, 1180 (2016).
- [40] A. B. Pippard, *Magnetoresistance in Metals*. Cambridge Studies in Low temperature Physics 2, Cambridge University Press (1989).
- [41] Z. Zhu, B. Fauqué, Y. Fuseya, and K. Behnia, *Angle-resolved Landau spectrum of electrons and holes in bismuth*, Phys. Rev. B **84**, 115137 (2011).
- [42] M. E. Peskin, and D. V. Schroeder, *An Introduction to Quantum Field Theory*, (Addison-Wesley, 1995).
- [43] K. Fujikawa, H. Suzuki, *Path Integrals and Quantum Anomalies*, (Clarendon Press, 2004).
- [44] S. Adler, *Axial-Vector Vertex in Spinor Electrodynamics*, Phys. Rev. **177**, 2426 (1969).
- [45] J. S. Bell and R. A. Jackiw, *A PCAC puzzle: $\pi_0 \rightarrow \gamma\gamma$ in the σ -model*, Nuovo Cimento A **60**, 47 (1969).
- [46] V. Aji, *Adler-Bell-Jackiw anomaly in Weyl semi-metals: Application to Pyrochlore Iridates*, Phys. Rev. B **85**, 241101 (2012).
- [47] D. T. Son, and B. Z. Spivak, *Chiral anomaly and classical negative magnetoresistance of Weyl metals*, Phys. Rev. B **88**, 104412 (2013).
- [48] S. A. Parameswaran, T. Grover, D. A. Abanin, D. A. Pesin, and A. Vishwanath, *Probing the Chiral Anomaly with Nonlocal Transport in Three-Dimensional Topological Semimetals*, Phys. Rev. X, **4**, 031035 (2014).
- [49] E. V. Gorbar, V. A. Miransky, and I. A. Shovkovy, *Chiral anomaly, dimensional reduction, and magnetoresistivity of Weyl and Dirac semimetals*, Phys. Rev. B **89**, 085126 (2014).
- [50] Burkov, A. A. *Chiral Anomaly and Diffusive Magnetotransport in Weyl Metals*, Phys. Rev. Lett. **113**, 247203 (2014).
- [51] T. Osada, *Negative Interlayer Magnetoresistance and Zero-Mode Landau Level in Multilayer Dirac Electron Systems*, J. Phys. Soc. Jpn. **77**, 084711 (2008).
- [52] A. A. Zyuzin, and A. A. Burkov, *Topological response in Weyl semimetals and the chiral anomaly*, Phys. Rev. B **86**, 115133 (2012).
- [53] A. G. Grushin, *Consequences of a condensed matter realization of Lorentz-violating QED in Weyl semi-metals*, Phys. Rev. D **86**, 045001 (2012).
- [54] P. Goswami, and S. Tewari, *Axionic field theory of (3+1)-dimensional Weyl semimetals*, Phys. Rev. B **88**, 245107 (2013).
- [55] K. Fukushima, D. E. Kharzeev, H. J. Warringa, *The Chiral Magnetic Effect*, Phys. Rev. D **78**, 074033 (2008).
- [56] M. M. Vazifeh, M. Franz, *Electromagnetic Response of Weyl Semimetals*, Phys. Rev. Lett. **111**, 027201 (2013).
- [57] Y. Chen, Si Wu, A. A. Burkov, *Axion response in Weyl semimetals*, Phys. Rev. B **88**, 125105 (2013).
- [58] G. Xu, H. Weng, Z. Wang, X. Dai, and Z. Fang, *Chern Semimetal and the Quantized Anomalous Hall Effect in $HgCr_2Se_4$* , Phys. Rev. Lett. **107**, 186806 (2011).
- [59] G. Y. Cho, *Possible topological phases of bulk magnetically doped Bi_2Se_3 : turning a topological band insulator into the Weyl semimetal*, arXiv:1110.1939 (2011).
- [60] B. Shen, X. Deng, G. Kotliar, and N. Ni, *Fermi surface topology and negative longitudinal magnetoresistance observed in the semimetal $NbAs_2$* Phys. Rev. B **93**, 195119 (2016).
- [61] S.-B. Zhang, H.-Z. Lu, and S.-Q. Shen, *Linear magnetoconductivity in an intrinsic topological Weyl semimetal*, New J. Phys. **18**, 053039 (2016).
- [62] C. Z. Chen, H.-W. Liu, H. Jiang, and X.-C. Xie, *Positive magnetoconductivity of Weyl semimetals in the ultraquantum limit*, Phys. Rev. B **93**, 165420 (2016).
- [63] Y.-W. Sun, and Q. Yang, *Negative magnetoresistivity in holography*, arXiv:1603.02624 (2016).
- [64] B. Z. Spivak, and A. V. Andreev, *Magnetotransport phenomena related to the chiral anomaly in Weyl semimetals*, Phys. Rev. B **93**, 085107 (2016).
- [65] D. A. Pesin, E. G. Mishchenko, and A. Levchenko, *Density of states and magnetotransport in Weyl semimetals with long-range disorder*, Phys. Rev. B **92**, 174202 (2015).
- [66] A. Jimenez-Alba, K. Landsteiner, Y. Liu, and Y.-W. Sun, *Anomalous magnetoconductivity and relaxation times in holography*, J. High Energy Phys. **2015**, 1 (2015).
- [67] A. A. Burkov, *Negative longitudinal magnetoresistance in Dirac and Weyl metals*, Phys. Rev. B **91**, 245157 (2015).
- [68] V. A. Zyuzin, *Magnetotransport of a Weyl semimetal within kinetic equation approach*, arXiv:1608.01286
- [69] H.-J. Kim, K.-S. Kim, J. F. Wang, M. Sasaki, N. Satoh, A. Ohnishi, M. Kitaura, M. Yang, and L. Li, *Dirac versus Weyl Fermions in Topological Insulators: Adler-Bell-Jackiw Anomaly in Transport Phenomena*, Phys. Rev. Lett. **111**, 246603 (2013).
- [70] Q. Li, D. E. Kharzeev, C. Zhang, Y. Huang, I. Pletikoscic, A. V. Fedorov, R. D. Zhong, J. A. Schneeloch, G. D. Gu, T. Valla, *Observation of the chiral magnetic effect in $ZrTe_5$* , arXiv:1412.6543 (2014).
- [71] N. Tajima, S. Sugawara, R. Kato, Y. Nishio, and K. Kajita, *Effects of the Zero-Mode Landau Level on Inter-Layer Magnetoresistance in Multilayer Massless Dirac Fermion Systems*, Phys. Rev. Lett. **102**, 176403 (2009).
- [72] N. Kikugawa, P. Goswami, A. Kiswandhi, E. S. Choi, D. Graf, R. E. Baumbach, J. S. Brooks, K. Sugii, Y. Iida, M. Nishio, S. Uji, T. Terashima, P. M. C. Rourke,

- N. E. Hussey, H. Takatsu, S. Yonezawa, Y. Maeno, and L. Balicas, *Interplanar coupling-dependent magnetoresistivity in high-purity layered metals*, Nature Commun. **7**, 10903 (2016).
- [73] C. Shekhar, F. Arnold, S.-C. Wu, Y. Sun, M. Schmidt, N. Kumar, A. G. Grushin, J. H. Bardarson, R. D. dos Reis, M. Naumann, M. Baenitz, H. Borrmann, M. Nicklas, E. Hassinger, C. Felser, and B. Yan, *Large and unsaturated negative magnetoresistance induced by the chiral anomaly in the Weyl semimetal TaP*, arXiv:1506.06577 (2015).
- [74] Y.-Y. Wang, Q.-H. Yu, P.-J. Guo, K. Liu, and T.-L. Xia, *Resistivity plateau and extremely large magnetoresistance in NbAs₂ and TaAs₂*, Phys. Rev. B **94**, 041103 (2016).
- [75] H. Wang, C.-K. Li, H. Liu, J. Yan, J. Wang, J. Liu, Z. Lin, Y. Li, Y. Wang, L. Li, D. Mandrus, X. C. Xie, J. Feng, and J. Wang, *Chiral anomaly and ultrahigh mobility in crystalline HfTe₅*, Phys. Rev. B **93**, 165127 (2016).
- [76] G. Zheng, J. Lu, X. Zhu, W. Ning, Y. Han, H. Zhang, J. Zhang, C. Xi, J. Yang, H. Du, K. Yang, Y. Zhang, and M. Tian, *Transport evidence for the three-dimensional Dirac semimetal phase in ZrTe₅*, Phys. Rev. B **93**, 115414 (2016).
- [77] Y. Zhao, H. Liu, C. Zhang, H. Wang, J. Wang, Z. Lin, Y. Xing, H. Lu, J. Liu, Y. Wang, S. Jia, X. C. Xie, and J. Wang, *Anisotropic Fermi Surface and Quantum Limit Transport in High Mobility 3D Dirac Semimetal Cd₃As₂*, arXiv:1412.0330 (2014).
- [78] J. Xiong, S. K. Kushwaha, T. Liang, J. W. Krizan, W. Wang, R. J. Cava, and N. P. Ong, *Signature of the chiral anomaly in a Dirac semimetal: a current plume steered by a magnetic field*, arXiv:1503.08179 (2015).
- [79] T. Liang, Q. D. Gibson, M. N. Ali, M. Liu, R. J. Cava, and N. P. Ong, *Ultrahigh mobility and giant magnetoresistance in the Dirac semimetal Cd₃As₂*, Nat. Mater. **14**, 280 (2015).
- [80] X. Huang, L. Zhao, Y. Long, P. Wang, D. Chen, Z. Yang, H. Liang, M. Xue, H. Weng, Z. Fang, X. Dai, and G. Chen, *Observation of the chiral anomaly induced negative magneto-resistance in 3D Weyl semi-metal TaAs*, Phys. Rev. X **5**, 031023 (2015).
- [81] C. Zhang, S.-Y. Xu, I. Belopolski, Z. Yuan, Z. Lin, B. Tong, N. Alidoust, C.-C. Lee, S.-M. Huang, H. Lin, M. Neupane, D. S. Sanchez, H. Zheng, G. Bian, J. Wang, C. Zhang, T. Neupert, M. Z. Hasan, and S. Jia, *Observation of the Adler-Bell-Jackiw chiral anomaly in a Weyl semimetal*, arXiv:1503.02630 (2015).
- [82] S. Wiedmann, A. Jost, B. Fauqué, J. van Dijk, M. J. Meijer, T. Khouri, S. Pezzini, S. Grauer, S. Schreyeck, C. Brüne, H. Buhmann, L. W. Molenkamp, and N. E. Hussey, *Anisotropic and strong negative magnetoresistance in the three-dimensional topological insulator Bi₂Se₃*, Phys. Rev. B **94**, 081302(R) (2016).
- [83] H. B. Nielsen and M. Ninomiya, *The Adler-Bell-Jackiw Anomaly and Weyl Fermions in a Crystal*, Phys. Lett. B **130**, 389 (1983).
- [84] P. N. Argyres and E. N. Adams, *Longitudinal Magnetoresistance in the Quantum Limit*, Phys. Rev. **104**, 900 (1956).
- [85] P. Goswami, J. H. Pixley, and S. Das Sarma, *Axial anomaly and longitudinal magnetoresistance of a generic three-dimensional metal*, Phys. Rev. B **92**, 075205 (2015).
- [86] N. W. Ashcroft, N. D. Mermin, *Solid State Physics*, Cengage Learning; 1 edition (January 2, 1976).
- [87] S. Hikami, A. I. Larkin, and Y. Nagaoka, *Spin-Orbit Interaction and Magnetoresistance in the Two-Dimensional Random System*, Prog. Theor. Phys. **63**, 707 (1980).
- [88] G. Bergmann, *Weak Localization in thin films a time-of-flight experiment with conduction electrons*, Phys. Rep. **107**, 1 (1984).
- [89] Y. Imry and S.-k. Ma, *Random-Field Instability of the Ordered State of Continuous Symmetry*, Phys. Rev. Lett. **35**, 1399 (1975).
- [90] S. Bera, J. D. Sau, and B. Roy, *Dirty Weyl semimetals: Stability, phase transition and quantum criticality*, Phys. Rev. B **93**, 201302 (2016).
- [91] P. Goswami, A. H. Nevidomskyy, *Topological Weyl Superconductor to Diffusive Thermal Hall Metal Crossover in the B-Phase of UPt₃*, Physical Review B, **92**, 214504 (2015).
- [92] B. Roy and J. D. Sau, *Magnetic catalysis and axionic charge-density-wave in Weyl semimetals*, Phys. Rev. B **92**, 125141 (2015).
- [93] Q. Chen and G. A. Fiete, *Thermoelectric transport in double-Weyl semimetals*, Phys. Rev. B **93**, 155125 (2016).
- [94] D. Yoshioka and H. Fukuyama, *Electronic Phase Transition of Graphite in a Strong Magnetic Field*, J. Phys. Soc. Jpn. **50**, 725 (1981).
- [95] A. Bardasis and S. Das Sarma, *Peierls instability in degenerate semiconductors under strong external magnetic fields*, Phys. Rev. B **29**, 780 (1984).
- [96] A. H. MacDonald and G. W. Bryant, *Strong-magnetic-field states of the pure electron plasma*, Phys. Rev. Lett. **58**, 515 (1989).
- [97] X. Li, B. Roy, S. Das Sarma, *Spontaneous symmetry breaking and quantum Hall valley ordering on the surface of topological hexaborides*, Phys. Rev. B **92**, 235144 (2015).
- [98] X. Li, F. Zhang, and A. H. MacDonald, *SU(3) Quantum Hall Ferromagnetism in SnTe*, Phys. Rev. Lett. **116**, 026803 (2016).
- [99] X. Li, F. Zhang, Q. Niu, and A. H. MacDonald, *Spontaneous layer-pseudospin domain walls in bilayer graphene*, Phys. Rev. Lett. **113**, 116803 (2014).
- [100] B. Roy, and I. F. Herbut, *Unconventional superconductivity on honeycomb lattice: the theory of Kekule order parameter*, Phys. Rev. B **82**, 035429 (2010).
- [101] V. A. Miransky, I. A. Shovkovy, *Quantum field theory in a magnetic field: From quantum chromodynamics to graphene and Dirac semimetals*, Physics Reports **576**, 1 (2015).
- [102] B. Roy, M. P. Kennett, S. Das Sarma, *Chiral symmetry breaking and the quantum Hall effect in monolayer graphene*, Phys. Rev. B **90**, 201409 (2014).
- [103] J. C. Slonczewski and P. R. Weiss, *Band structure of Graphite*, Phys. Rev. **109**, 272 (1958).
- [104] J. W. McClure, *Band Structure of Graphite and de Haas-van Alphen Effect*, Phys. Rev. **108**, 612 (1957).
- [105] B. Fauqué, D. LeBoeuf, B. Vignolle, M. Nardone, C. Proust, K. Behnia, *Two phase transitions induced by a magnetic field in graphite*, Phys. Rev. Lett. **110**, 266601 (2013).
- [106] E. H. Hwang, S. Adam, and S. Das Sarma, *Carrier*

Transport in Two-Dimensional Graphene Layers, Phys. Rev. Lett. **98**, 186806 (2007); S. Adam, E. H. Hwang, V. M. Galitski, and S. Das Sarma, *A self-consistent theory for graphene transport*, Proc. Natl. Acad. Sci. USA **104**, 18392 (2007); Y.-W. Tan, Y. Zhang, K. Bolotin, Y. Zhao, S. Adam, E. H. Hwang, S. Das Sarma, H. L. Stormer, and P. Kim, *Measurement of Scattering*

Rate and Minimum Conductivity in Graphene, Phys. Rev. Lett. **99**, 246803 (2007); J.-H. Chen, C. Jang, S. Adam, M. S. Fuhrer, E. D. Williams, and M. Ishigami, *Charged-impurity scattering in graphene*, Nat. Phys. **4**, 377 (2008).